Thermal State of Sn-Pb Droplets in the Droplet-Based Manufacturing Process

by

Sucharita Sahu

S.B., Mechanical Engineering, 1992
Massachusetts Institute of Technology

Submitted to the Department of Mechanical Engineering
in Partial Fulfillment of the Requirements for the
Degree of Master of Science

at the

Massachusetts Institute of Technology
May 1994

© Massachusetts Institute of Technology 1994
All rights reserved

Signature of Author .....
Department of Mechanical Engineering
May 6, 1994

Certified by .....
Jung-Hoon Chun
Edgerton Assistant Professor of Mechanical Engineering
Thesis Supervisor

Accepted by .....
Ain Ants Sonin
Professor of Mechanical Engineering
Chairman, Mechanical Engineering Committee on Graduate Thesis

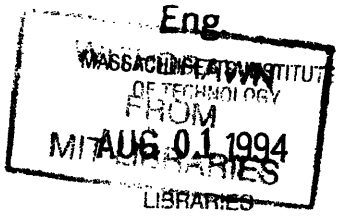

Abstract

Thermal State of Sn-Pb Droplets in the
Droplet-Based Manufacturing Process

by

Sucharita Sahu

Submitted to the Department of Mechanical Engineering
on May 6, 1994
in Partial Fulfillment of the Requirements for the
Degree of Master of Science

Abstract

This work characterizes the thermal state of Sn-Pb droplets during a droplet-based manufacturing process called the uniform-droplet spray process. We have designed and fabricated an in-situ calorimetric device to investigate the thermal state of Sn-5wt%Pb, Sn-25wt%Pb, and Sn-37wt%Pb droplets. Under equilibrium conditions, the thermal state of the droplets is defined by the temperature and liquid fraction of the droplets. Under non-equilibrium conditions, the thermal state of the droplets is defined by the temperature, liquid fraction, and prior undercooling of the droplets. The main factors affecting the thermal state of individual droplets in the uniform-spray process are flight distance between the orifice and the substrate, gas atmosphere in the uniform droplet apparatus, and composition of the alloy. From the microstructures of the collected powders, the relationships between the thermal state of the droplets and the morphologies of the droplets are deduced. A scanning electron microscopic analysis on Sn-5wt%Pb droplets shows the effects of temperature, enthalpy, and liquid fraction on the shape of the solidification front inside the droplets for the uniform-droplet spray process. The enthalpies of Sn-5wt%Pb droplets collected at different flight distances are determined through experimental measurements using the calorimetric device. The measured droplet enthalpies are compared with enthalpies calculated using an equilibrium solidification model.

Thesis Supervisor: Jung Hoon Chun
Title: Edgerton Assistant Professor of Mechanical Engineering

Acknowledgments

At the very outset, I want to thank Jung-Hoon Chun for his support and guidance. His professional advice and personal understanding have been invaluable. I also want to thank Teiichi Ando for his contributions to this work. I benefitted greatly from our discussions.

Many thanks to all my research group members: Godard Abel, Paul Acquaviva, Chen-An Chen, Randy Hyun, Tom Nowak, Wesley Williams, and Pyongwon Yim for the valuable discussions. I thank Gretchen Cuda for helping me with the metallographic work.

Among many other individuals who have helped me during my work are Yinlin Xie, Fred Cote, Mina Yang and Diane DeAlderete. A special thanks to all of them. I would also like to thank Pratyush Kumar for all his support and help. I fondly dedicate this work to my parents: Kailas Chandra Sahu and Bimala Sahu.

Contents

List of Figures

List of Tables

List of Symbols

H_d	Enthalpy of the droplets (J)
H_l	Enthalpy loss (J)
m_d	Mass of the droplets (kg)
m_o	Mass of the oil (kg)
c_d	Specific heat of the droplets (J/kg °C)
T	Temperature (°C)
t	Time (s)
c_o	Specific heat of the oil (J/kg °C)
f	Mass flow rate (kg/s)
P_o	Power input during calibration experiments (W)
Δh_d	Enthalpy difference per droplet before and after the droplet enters the oil (J/droplet)
ΔH_d	Enthalpy difference of all the droplets before and after the droplets enter the oil (J)
T_i	Temperature at the beginning of the experiment (°C)
T_f	Temperature at the end of the experiment (°C)
t_i	Time at the beginning of the experiment (s)
t_f	Time at the end of the experiment (s)
V_d	Volume of the droplets (m^3)
ρ_d	Density of the droplets (kg/m^3)
n	Number of droplets entering the oil
ΔT	Undercooling (°C)
ΔH_f	Enthalpy of fusion (J/kg)
x	Liquid fraction

CHAPTER 1 Introduction: An Overview of the Droplet-Based Manufacturing Process

1.1 Introduction to Spray Forming

Spray forming is a single step Droplet-Based Manufacturing (DBM) process that is used to create a variety of parts [5, 8, 13]. In this process, a stream of molten metal or molten alloy is broken into a spray of droplets which are collected on a substrate to form a part. Figure 1.1 shows a schematic of the spray forming process [19]. Usually, the molten alloy or metal stream is broken down into a spray of droplets by a method called "gas atomization". During gas atomization, a high velocity gas jet is directed towards the stream to break it up into randomly sized droplets. Some of the parts that can be produced by this process include simple near-net shapes, such as cylinders, disks, and sheets [8, 12]. The shape of the part is determined by the shape of the substrate and the relative motion between the spray and the substrate. Spray forming has several advantages over other competing processes such as casting. Some of the advantages are listed below:

1. It is a quick process.
2. It can create parts that have a desirable microstructure. A desirable microstructure is characterized by a uniform distribution of equiaxed grains, an uniform distribution of second phases, and an absence of pores.

The above characteristics allow spray forming processes to form parts that have tailored mechanical properties. Examples of the variety of parts that can be produced using spray forming processes are tubes and sheets from special steels, superalloys, aluminum, and copper using the Osprey Preform Process which is a gas atomization process [19].

1.2 Limitations of Conventional Spray Forming Processes

The success of the spray forming process is gauged by several attributes: control of deposit microstructure, control of deposit shape, and maximization of process yield [6, 7]. Since the deposit is created by individual droplets, the properties of the droplets are among the principal factors affecting the properties of the deposit. As an example, the

size of the droplets determines the thermal state and the morphology of the atomized droplets at the time of deposition. This is because the size directly affects the amount of heat transferred from the droplet to the ambient gas and the acceleration and deceleration of the droplets during their flight towards the substrate. In other words, the size affects the mass and enthalpy of the droplets and therefore it has a significant effect on the thermal state and morphology attained by the droplets. Sprays consisting of non-uniform droplets imply a random distribution of mass fluxes, enthalpy fluxes and morphological states of the droplets which are transferred in the same random manner to the deposit. Due to this randomness, the microstructure of the deposit is non-uniform.

The non-uniformity in the size of the droplets also affects the repeatability of the experiments carried out to understand and characterize spray forming [19]. This is because each point in the spray contains different mass and enthalpy fluxes and different distributions of droplet sizes, velocities, and enthalpies. These variations make it difficult to characterize the state of the section of the spray responsible for creating a portion of the deposit. Therefore, the first drawback of conventional spray forming processes is the production of non-uniform droplets.

The second drawback is the existence of a high degree of coupling between the variables in the spray forming process [9, 11]. As an example, a change of the gas flow rate that breaks the molten alloy stream into droplets can change several variables at the same time. Some of these variables include droplet impact velocity, droplet cooling rate, and deposit cooling rate. It thus becomes difficult to understand and determine how the gas flow rate affects one of the variables alone, for example, the droplet impact velocity. This difficulty leads to a severe limitation of the range of experiments that can be carried out using the spray forming process.

The two drawbacks mentioned above were some of the reasons that motivated the introduction of a spray forming process that produces an uniform-droplet spray (UDS) of metal. It was argued that the production of uniform droplets would eliminate many, if not all of the above drawbacks [19].

1.3 Introduction to the Uniform-Droplet Spraying Process

This section describes the mechanism by which uniform droplets are produced and directed to form a deposit in the uniform-droplet spraying process. Section 2.2 gives a detailed explanation of the apparatus and the role of individual parts of the apparatus used to create the droplets. Section 2.3 describes the step by step procedure used to create the droplets using the apparatus. Figure 2.1 shows a schematic of the uniform

droplet generator that is used to create the droplets and produce the deposit. This apparatus produces uniform, electrically charged droplets which are collected on a substrate to produce a part. The apparatus is based on the same concept that is used in continuous ink-jet printers [21]. However, the apparatus is designed to work with metals and alloys as well as to prevent the coalescence of droplets at large flight distances.

The molten metal or alloy stream is broken into droplets due to Rayleigh instability imposed on the jet stream. Rayleigh instability criterion explains that over time, a laminar jet stream will break up into droplets because the surface energy per volume is lower for spheres than for cylinders. A jet typically will break at random intervals around a preferred wavelength to form non-uniform droplets [1]. However, it is possible to break the jet into uniform droplets by imposing periodic vibrations of sufficient amplitude at the base of the jet [1, 2, 21]. These periodic vibrations override the random disturbances responsible for creating non-uniform droplets and break up the stream into uniform droplets.

The uniform droplets are prevented from coalescence with each other during flight by being electrically charged with the same polarity. The repelling action enables the droplets to arrive individually at the substrate. Experiments have shown that a charge of 10^{-12} coulombs/droplet helps in preventing coalescence for a flight distance of about 500 mm [19]. The flight distance is the distance between the orifice through which the molten stream is forced out and the substrate where the droplets are intercepted to form the deposit.

The spray consists of charged droplets that scatter as they fly towards the substrate to form a deposit. The rate of scattering is controlled by varying the amount of charge on the droplets. The consolidation of the charged droplets on the substrate forms a deposit. One of the principal factors that controls the level of consolidation of the droplets is the amount of liquid fraction carried by each individual droplet when it hits the substrate. If the droplets in the spray contain too much solid, the deposit will be porous. At the same time, the process yield is reduced since many of the droplets will bounce instead of sticking to the deposit. On the other hand, if the droplets in the spray contain too much liquid, they will merge with each other to form a liquid pool on the substrate. This pool will eventually solidify to form a coarse, segregated microstructure in the deposit. The concentration and distribution of the different phases in the solidification structure will determine the solidification parameters within the deposit such as dendritic arm spacing [19].

1.4 Advantages of the Uniform-Droplet Spray Process

Some of the initial observations show that the uniform-droplet spray process can provide many advantages which include most of the advantages offered by spray forming [10, 19]. The significant advantages are characterized in terms of higher yields, deposit microstructure, control and repeatability of experiments, complex part formation, de-coupling of system parameters, modeling of system variables, ease of experimentation, and processing of novel materials. The use of uniform droplets offers these advantages in the following manner:

1. Deposit Microstructure: Uniform droplets share identical velocities, temperatures, liquid fractions, and undercooling at any given flight distance. The wide distributions of velocities, temperatures, and liquid fractions observed in conventional spray processes are absent in the uniform-droplet spray process. This enables the deposit to have a uniform mass flux and enthalpy flux in the latter process which then helps to form a deposit microstructure that is uniform and homogenous. By careful control of the thermal states of the droplets, the microstructures can develop as fine-equiaxed and homogenous with low porosity levels.
2. Decoupling of system variables: Unlike gas-atomized spray-forming, uniform-droplet spray process is a de-coupled design. Each system variable can be made independent of the other system variables. Through experiments, relationships between the different system variables have been defined and characterized. As an example, the spread of the spray is controlled primarily by the charging amount imparted to the droplets. Therefore, if a deposit requires a larger spread area, the charge carried by the droplets is increased. It is then possible to predict and confirm how a variation in system variables can affect the deposit produced. This information has advantages in terms of modeling and characterizing the system as well as in terms of controlling and repeating the experiments.
3. Characterization of the process: An absence of randomness in size enables the process to be characterized in a systematic manner. As an example, experiments have been performed to measure the enthalpy of each droplet in the system. This is essential to determine the thermal state of the droplets, which is difficult in conventional spray forming processes where all the droplets have different enthalpies. Experiments have also been performed to determine the velocity and charge of individual droplets during the droplet-based manufacturing process.

1.5 Characterization of the Uniform-Droplet Spray Process

The potential of droplet-based manufacturing processes can be exploited fully after a thorough understanding of the process is achieved. Several mechanisms need to be understood individually before the process can be completely characterized. These mechanisms include fundamentals concerning the following: how the molten stream breaks into uniform droplets, what is the effect of oxidation on the break-up of the molten stream, how the droplets are charged, how the droplets interact during their flight towards the substrate as a result of being charged, how the droplets consolidate to form the deposit, and finally, how the properties of the deposit are controlled and formed. Besides understanding the process, there are two other motivating factors for understanding the fundamentals of the above mechanisms. The first factor is to create a deposit that has a homogenous, non-porous and fine-equiaxed morphology. The second factor is to create deposits with novel morphologies which can be used for specific applications. As an example, a deposit grown with a specific morphology along one of its dimensions can have a certain property strengthened along that dimension. One of the principal factors controlling the properties of the deposit is the microstructure of the deposit. Previous studies [17, 19] have indicated that the deposit microstructure depends on several factors. These factors are the thermal state of the droplets, the fluxes of the droplets, the impact states of the individual droplets, the thermal conditions at the substrate-deposit interface, and the processing conditions of the experiments.

This work attempts to understand and characterize one of the factors responsible for controlling and forming deposit microstructures [15, 16]. This factor is the thermal state of the droplets. Specifically, this study is carried out first to understand the thermal state of the droplets and second, to determine how the thermal state of the droplets affects the microstructure of the deposit.

To summarize, it is critical to understand how and why the thermal state of the droplets affects the microstructure of the deposit for three fundamental reasons:

1. To characterize the process-structure relationship in the uniform-droplet spray process.
2. To control the microstructure of the deposit and thereby control the properties of the parts produced from the deposit.
3. To create novel microstructures of the deposit for specific applications.

1.6 Research Objectives

The thermal state of the droplets is one of the principal factors that controls the microstructure of the deposit in the uniform-droplet spray process. When the droplets undergo equilibrium solidification, their thermal state is defined by their temperature and their liquid fraction or their enthalpy and their liquid fraction. During equilibrium solidification, each droplet starts solidifying at its liquidus temperature and completes solidifying at its solidus temperature. When the droplets undergo non-equilibrium solidification, their thermal state is defined by their temperature, liquid fraction and undercooling or their enthalpy, liquid fraction and undercooling. During non-equilibrium solidification, droplets start solidifying at a temperature lower than their liquidus temperature. The difference between the temperature at the start of solidification and their liquidus temperature is called the undercooling.

Therefore, a complete understanding of the thermal state of the droplets requires a study of both equilibrium solidification (with no undercooling) and non-equilibrium solidification (with undercooling).

Previous studies have investigated the thermal state of the droplets under equilibrium solidification conditions. Specifically, work has been done to study the relationships between the thermal state of the droplets and the microstructure of the deposit. At the same time, the temperature, enthalpy and liquid fraction of the droplets have been measured during experiments assuming equilibrium conditions and compared with values derived from an equilibrium model [19].

This work investigates additional aspects of the thermal states of the droplets. They are as follows:

1. External factors affecting the thermal state of the droplets in the droplet-based manufacturing processes. These factors include system variables like the flight distance at which the droplets are collected and the type of inert gas through which the droplets travel. The factors are investigated under both equilibrium and non-equilibrium solidification conditions.
2. Relationship between each factor affecting the thermal state of the droplets and the morphology of the droplets. The droplets are quenched in oil and collected in a calorimeter (Section 2.2). Experiments are carried out to decouple the factors affecting the thermal state of the droplets and to study the effect of each factor on the morphology of the droplets.

3. Initiation of the solidification process within an individual droplets as a result of quenching. (2) and (3) are important parameters needed to characterize how external processing conditions (system variables) interact with internal (occurring within the droplet) microstructural evolution conditions to create the microstructure of the droplets.
4. Measurement of the enthalpy of an individual droplet assuming non-equilibrium conditions. This was motivated in order to determine the undercooling of an individual droplet. A detailed description of how the enthalpy of a droplet is related to the undercooling of the droplet is qualitatively given in Section 2.3. When the droplets undergo non-equilibrium solidification, their thermal state is defined by their enthalpy, liquid fraction and undercooling. Potentially, the liquid fraction of the droplet can be determined within an approximation from metallographic studies by comparing the proportions of solid and liquid phases. Therefore, the entire thermal state of an undercooled individual droplet can be determined quantitatively by using the procedure described in this work.
5. As a future work, a model [18] is being developed to explain how the thermal state (temperature, enthalpy, liquid fraction) and the internal solidification parameters (solid-liquid interface velocity, solid-liquid interface composition, dendritic tip radius) of an undercooled droplet can be determined theoretically. This model is a modification of the Lipton-Glicksman-Kurz (LGK) model [20]. It modifies the LGK model by introducing kinetic undercooling that results from the high solid-liquid interface velocity occurring within the droplet. Similar models accounting for the kinetic undercooling have been presented [18,24,25].

1.7 Approach

To investigate the thermal states of the droplets in flight, three different Sn-Pb alloys were studied. At the same time, an in-situ calorimetric apparatus was built to analyze the thermal states in flight.

Three different Sn-Pb alloys were used to investigate the thermal state of the droplets. They are Sn-5wt%Pb, Sn-25wt%Pb and Sn-37wt%Pb (Figure 1.2). These alloys were used because of several reasons. First, a literature survey shows that these specific Sn-Pb alloys have been studied extensively in spray forming processes to understand fundamental solidification phenomena [16]. By comparing the morphologies of Sn-Pb powders obtained in this work with the morphologies of Sn-Pb powders pro-

duced in other studies, we can understand how the uniform-droplet spray process is different from conventional spray forming processes and whether the uniform-droplet spray process is capable of producing any results not previously obtained. Second, the three alloys cover a wide range of Pb-content and can therefore help in the characterization of wide compositions of Sn-Pb alloys in general. Third, Sn-25wt%Pb and Sn-37wt% alloys were specifically used to study the relationship between the thermal states of the droplets and the morphology of the droplets. This is because alloys having a Pb content higher than 20% yield a Pb-rich phase as the primary phase when solidified after a large undercooling [18, 22]. Therefore, by studying the solidification microstructure of the droplets, one can investigate the prior undercooling. Fourth, Sn-5wt%Pb was investigated to determine the enthalpy of an individual droplet in flight. This specific alloy was selected because theoretical models [18, 24, 25] which are currently being developed apply to dilute alloys.

An in-situ calorimetric apparatus was built to collect the uniform droplets during flight. It was used to investigate the factors affecting the thermal state of the droplets, the relationship between the thermal state of the droplets and the morphologies of the droplets, the initiation of the solidification front within the droplets and the measurement of the enthalpy of an individual droplet. This apparatus was designed as a modular unit of the existing uniform droplet generator system that is used to create the droplets. The calorimetric apparatus consists of three identical calorimeters or calorimetric devices. A detailed description of both the uniform droplet generator and the calorimetric apparatus is given in Chapter 2. The factors affecting the thermal state of the droplets, the relationship between the thermal state of the droplets and the morphologies of the droplets as well as the initiation of the solidification front within the droplets were determined by studying the morphologies of the quenched droplets in the calorimetric devices. The enthalpy of an individual droplet was determined by measuring the temperatures of the oil near the bottom and top of the calorimetric devices and by using these temperatures in an energy balance relationship. A detailed explanation of the procedures used is given in Chapter 2.

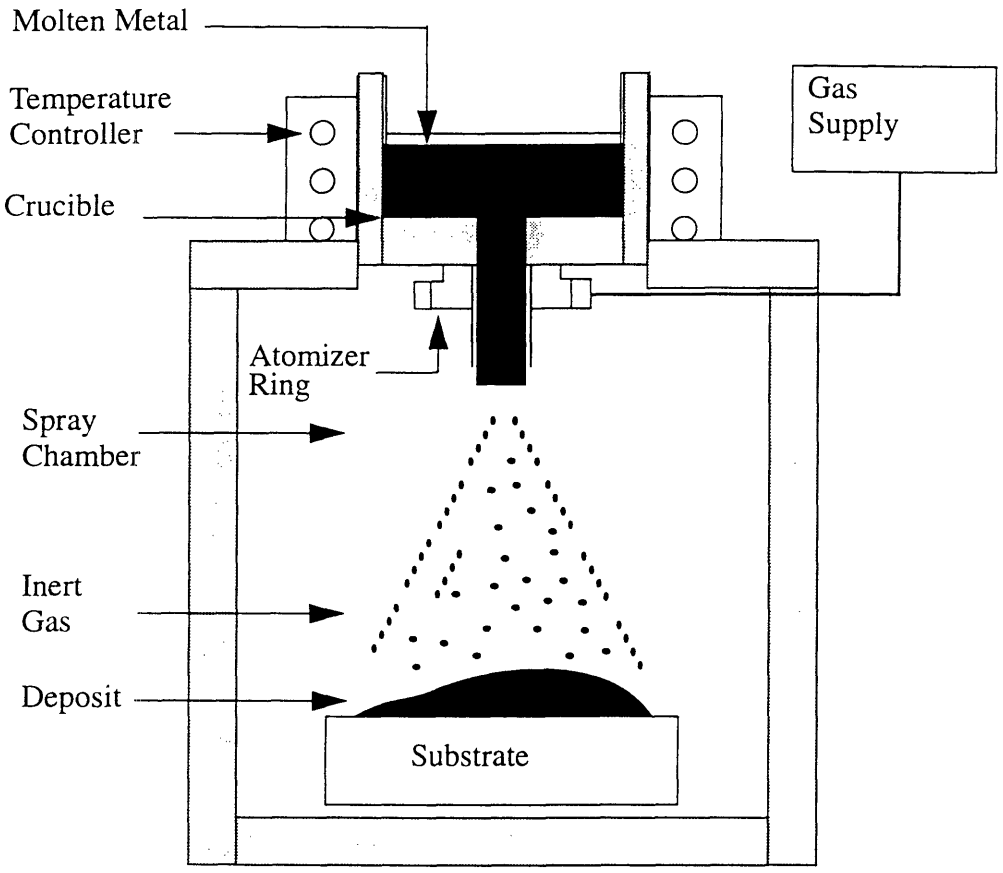

Figure 1.1 Schematic of the spray forming process.

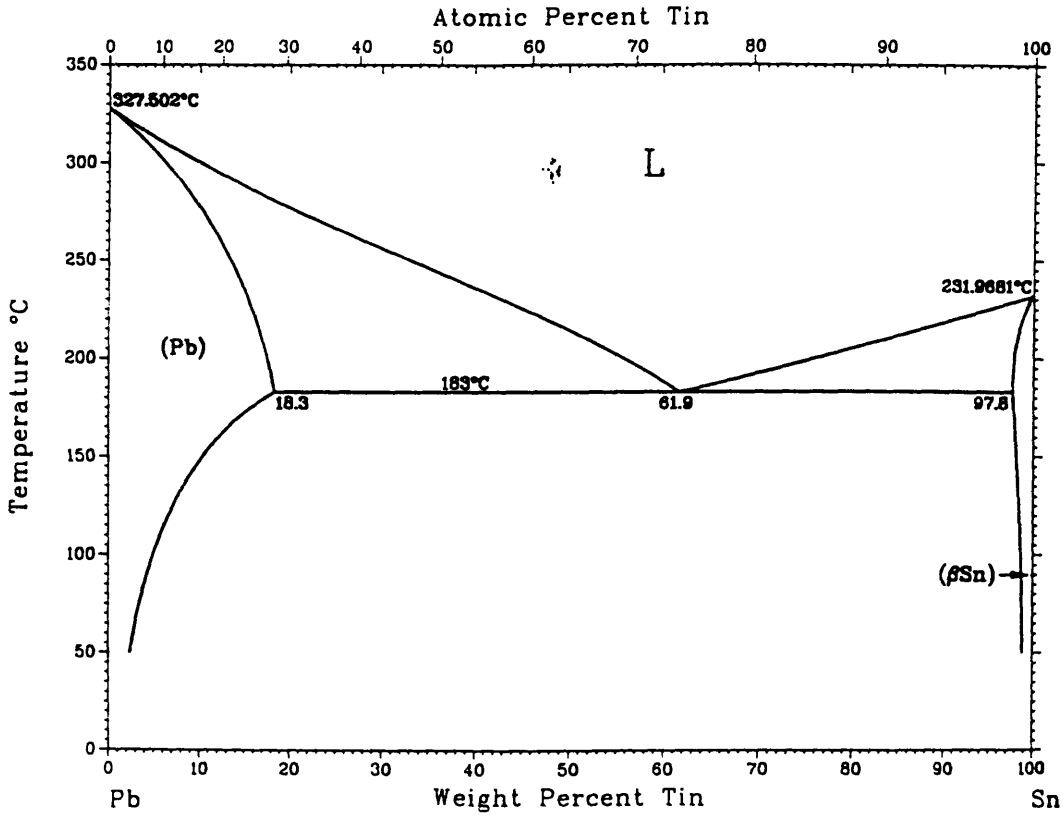

Figure 1.2 The Tin-Lead equilibrium phase diagram.

CHAPTER 2 Experiments

This chapter describes the experimental apparatus and the experimental procedure that were implemented to meet the objectives of this work. The main goals of this work are as follows:

1. Determination of system variables and conditions affecting the thermal state of the droplets.
2. Relationship between the thermal state of the droplets and the morphology of the droplets.
3. Initiation of solidification inside an individual droplet during flight. This aspect focuses on the shape of the solidification front inside a droplet quenched in oil and speculates on the origin of the nucleation sites inside the droplet.
4. Determination of the enthalpy of an individual droplet in flight.
5. Procedure to determine the undercooling of an individual droplet in flight. This section explains how the enthalpy data can be used to determine the undercooling amount of an individual droplet in flight.

Section 2.1 describes the experimental apparatus that was built to provide the optimum conditions needed to investigate and meet the goals. Section 2.2 describes the experimental procedure that was used to reach each goal. In Section 2.2, there is an overview of the alloys and the experiments as well as the experimental conditions and parameters involved for each experiment and each alloy.

2.1 Experimental Apparatus

The following sections describe the uniform droplet generator and the calorimetric apparatus that were used together to create the uniform Sn-5wt%Pb, Sn-25wt%Pb and Sn-37wt%Pb droplets and to study their thermal states. The droplet generator is an existing system that creates the uniform droplets [19]. The calorimetric apparatus was built specifically for this work in order to study the thermal state of the droplets in flight. It was designed as a modular unit of the droplet generator and supports the calorimetric devices in which the droplets are collected in oil during flight.

2.1.1 The uniform droplet generator

Figure 2.1 shows a schematic of the low temperature (< 500°C) uniform droplet generator system [19] with the modular calorimetric apparatus. The droplet generator is a

previously built system that creates uniform, electrically charged molten metal or alloy droplets. It consists of seven components: a crucible, an orifice, a spray chamber, a melt vibrating system, a droplet charging system and a monitoring system. Each part is briefly described below.

The *crucible* is machined from 303 stainless steel and can hold up to 500 ml of molten metal or alloy. The melt temperature inside the crucible is held constant to within 1°C using a temperature control system that has the following parts: a PID controller, a K-type thermocouple and a pair of 300 W band heaters (Omega: Stamford, CT). The *orifices* used in the experiments are 100 μm (Bird Precision: Waltham, MA) in diameter. They are drilled in ruby or sapphire (high purity Al_2O_3) jewels. They are mounted with Autostic, a ceramic adhesive in pockets that are machined on the bottom of the crucible. To attain directional stability of the jets, each orifice is modified to have a radius equivalent to 0.01 of its inner diameter at its entrance. The *spray chamber* is a hollow cylindrical chamber that is 900 mm long and 150 mm in inner diameter. It is made out of pyrex conical system pipe (Corning: Corning, NY). It holds the inert gas (N_2 or N_2-2%H_2). The *gas control system* maintains the inert gas environment in the spray chamber. It also forces the jet out of the orifice by applying a pressure differential between the crucible and the chamber. It consists of the following parts: two regulated gas supplies (a high pressure source operating at pressure levels between 200 to 550 kPa and a low pressure source operating at a pressure level of 35 kPa), a vacuum pump, and a three-way valve connecting the crucible to either the spray chamber or the high pressure source.

The *melt vibrating system* is responsible for producing perturbations at the orifice that break the jet at regular intervals to create uniform droplets. It consists of the following parts: a piezo-electric transducer, a function generator, an amplifier, a transformer, a shaft and disk assembly and a frequency counter. The piezo-electric crystal is a lead zirconate titanate (PZT-5A/Navy type II) and is 12.7 mm in diameter and 3.18 mm thick (Morgan Matroc: Bedford, OH). The function generator and amplifier along with the transducer drive the crystal between 400 volts and 1000 volts corresponding to a frequency between 5 and 30 kHz. The *droplet charging system* electrically charges the droplets so that they break away from the jet and repel each other during their flight towards the substrate. Therefore their coalescence is prevented during flight. The charging system consists of the following parts: a DC voltage source, a 6.35 mm thick brass plate with a 3.18 mm diameter hole. The *monitoring system* provides feedback for controlling the droplet size. It consists of the following parts: a video system equipped with a stroboscope (Quadtech: Bolton, MA), a micro-mac CCD video cam-

era (Techniquip: Hollywood, CA) and an unimac 0.7x to 4.5x power microscopic zoom lens (Meiji Techno: Woburn, MA).

2.1.2 The calorimetric apparatus

The calorimetric apparatus has been built specifically to study the thermal state of the droplets. It consists of three identical calorimetric devices mounted on two shafts attached to the lower plate system of the uniform droplet apparatus described above. The shafts are 700 mm and 600 mm in height. The calorimetric devices can be bolted to the shafts at any flight distance between 260 mm and 860 mm. The 600 mm long shaft can be rotated during the experiments if necessary. This permits the droplets to be collected individually in each of the three devices without being intercepted by the other two. A schematic of a calorimetric device is shown in Figure 2.2. Each device consists of a 5 ml capacity ceramic cup glued to a 25.4 mm by 76.2 mm by 6.35 mm aluminum plate. Ceramic cups are selected because they are good insulators and minimize heat loss during the experiments. Each cup is filled with 3 cc of Dow Corning 704 diffusion pump silicon oil (Dow Corning: Midland, MI). This oil was chosen because of several properties: it does not react with oxygen at operating temperatures and it is chemically inert with metal parts, seals and gases such as hydrogen and carbon monoxide. Droplets are intercepted in the oil bath as well as on the aluminium plate projection.

To measure the enthalpies of the droplets in flight, the same calorimetric apparatus is used with two modifications. The first modification is the introduction of thermocouples into the oil bath of each calorimetric device which are used to monitor the temperature of the oil. Two K-type Chromel-Alumel thermocouples (Omega: Stamford, CT) are inserted into the oil bath of each calorimetric device which is shown in Figure 2.2. One thermocouple is placed near the bottom of the bath and the other thermocouple is placed near the surface of the bath. They are used to monitor the temperatures near the bottom and the surface of the oil respectively. Two thermocouples are also used to monitor the temperature of the N_2 gas in the chamber during each experiment. The second modification is the introduction of a data acquisition system which is used to monitor the transient and steady state temperatures of the oil. The data acquisition system consists of the following parts: a Gateway 2000, 486 computer system (Gateway: N. Sioux City, SD), a DAS-TC PC board (Keithley Metrabyte: Taunton, MA) and DataLogger utility software (Keithley Metrabyte: Taunton, MA). The DAS-TC board and the DataLogger utility software monitor the transient and steady state temperatures of the thermocouples during the experiments. The eight thermocouples (two each for each of the three calorimetric devices and two for the N_2 gas) are

connected to the computer through connectors machined on the bottom plate of the droplet generator system.

The weight of the oil used to collect the droplets in the calorimetric devices and the weights of the collected droplets are measured using an electronic balance (Ohaus Corporation: Florham Park, NJ) and a dial-gram balance (Ohaus Corporation: Florham Park: NJ). In both cases the error associated with the measurements is ±0.05 gm.

2.2 Experimental Procedure

The following sections describe the procedures that were used to create the droplets and determine the thermal state of the droplets. Specifically, the sections describe the methods used to create the uniform droplets in the uniform droplet generator, determine the conditions affecting the thermal state of the droplets, determine the relationship between the thermal state of the droplets and the morphology of the droplets, study the initiation of solidification inside the droplets and measure the enthalpy of each droplet during its flight towards the substrate. The section concludes with the introduction of a method that can be used to evaluate the undercooling of the droplets from the measured enthalpy values of the droplets.

2.2.1 Production of uniform droplets

The parameters that were used to create the uniform droplets for each alloy are listed in Tables 2.1 and 2.2. The modular calorimetric apparatus was inserted into the uniform droplet generator apparatus (Figure 2.1). The whole system was sealed air-tight. The alloy was melted and allowed to reach a steady state, superheated value (50°C to 70°C above the melting point of the alloy). The spray chamber was then evacuated to 300 milli-torr and filled with an inert gas three times with the help of the gas control system. The three-way valve was then turned to disconnect the crucible from the spray chamber and to connect it to the high pressure source. The pressure differential between the crucible and the chamber was 136 kPa. The melt was forced out of the crucible through the orifice to form a laminar jet. The piezoelectric transducer in the melt vibrating system produced the right frequency to break the laminar stream into uniform droplets [1, 2, 3, 14]. The droplet charging system electrically charged the droplets as they broke away from the jet so that no coalescence was possible during flight. The combination of the applied voltage and the capacitance between the plate and the jet brought a charge to the tip of the jet. This charge was retained by each droplet as it travelled towards the substrate. These droplets were intercepted and collected during their flight by the calorimetric devices. Once the run was over, the calorimetric devices were removed and the weight of the droplets was measured using the dial-

gram balance. They were then prepared for metallographic studies in the metallographic laboratory.

2.2.2 Determination of the factors affecting the thermal state of the droplets

Sn-25wt%Pb and Sn-37wt%Pb were investigated to study the factors affecting the thermal state of the droplets in flight. The thermal state of the droplets in the uniform-droplet spray process was analyzed by studying the microstructures of the collected powders. The powders were collected in the calorimeter inside the uniform droplet generator. By analyzing their microstructures, the morphologies of the droplets were deduced. It was concluded that three factors affect the thermal state of the droplets in flight: flight distance between the orifice through which the spray is ejected and the substrate where the droplets are collected, type of inert gas used in the uniform droplet generator, and alloy composition.

The flight distance affects the temperature and liquid fraction of the droplets. As the distance between the orifice and the substrate increases, the temperature and the liquid fraction of the droplets decrease. Therefore, by studying the microstructures of the collected powders at different flight distances, relationships between the temperature, liquid fraction and morphologies of the droplets were determined.

The inert gas affects the undercooling of the droplets. Two inert gases were used in this work. They are N_2 and N_2-2%H_2. The use of N_2-2%H_2 enables the H_2 to react with the O_2 in the chamber. Therefore the potential for oxide to be formed on the surface of a molten alloy droplet (which can act as high potency heterogenous nucleation sites) is reduced. Prevention of oxidation is considered to promote droplet undercooling. Hence the use of N_2-2%H_2 increases the chances for undercooling. The use of N_2-2%H_2 gas combined with $CaSO_4$ as a desiccator provides a partial pressure ratio p_{H_2}/p_{H_2O} of about 3000, a value more than sufficient to prevent oxidation of molten Sn-Pb alloys [17]. Without H_2, however, oxidation can take place at oxygen potentials as low as $10^{-40} atm$ and thus could have readily occurred in the $CaSO_4$ desiccated N_2 gas. Therefore, it is conceivable that the droplets produced in N_2-2%H_2 gas were undercooled more than those produced in N_2 gas. By studying the microstructures of the collected powders produced under different inert gases, relationships between the undercooling and the morphologies of the droplets were determined.

The alloy composition affects the undercooling of the droplets [16]. The composition was varied between Sn-25wt%Pb and Sn-37wt%Pb. For purposes of comparison of morphologies, the two compositions had to be in the same range in terms of the Pb content (phase diagram, Figure 1.2). When the composition of Pb in Sn-Pb alloys is greater than 20%, a Pb-rich phase in formed both in the presence and absence of

undercooling [18]. Therefore, it is possible to compare the morphologies of Sn-25wt%Pb and Sn-37wt%Pb droplets by identifying their Pb-rich phases.

However, it has proved difficult to quantatively determine the difference in undercooling by looking at the microstructures of the collected droplets. Nevertheless, some important differences have been determined between the two alloy compositions in terms of the droplet liquid fraction and the rate of solidification.

2.3 Relationship between the thermal state of the droplets and the morphology of the droplets

The relationship between the thermal state of the droplets and the morphology of the droplets was determined by studying the microstructures of the collected powders.

Sn-25wt%Pb and Sn-37wt%Pb powders collected in oil were investigated to study the effects of temperature, liquid fraction, and undercooling of the droplets on the morphologies of the droplets. Experiments were performed to decouple the factors and study the effect of each factor on the droplet morphology. Therefore, in each experiment, there was only one variable which could be either temperature, liquid fraction, or undercooling that affected the morphologies of the droplets. During each experiment, the collected powders were collected in the in-situ calorimeter in the uniform droplet generator. Their microstructures were studied under all the conditions. Two experiments were performed for each of the two alloys: the first was carried out in N_2 gas environment and the second was carried out in N_2-2%H_2 gas environment. The background gases were allowed to flow through the chamber after being desiccated with $CaSO_4$. For each alloy, the uniform droplets were intercepted in oil at vertical distances of 200, 375, 400, 600, 700 mm. Table 2.1 lists the system parameters that were used during the experiments for both alloys.

Table 2.1 Experimental conditions for Sn-25wt%Pb and Sn-37wt%Pb

Alloy	Sn-25wt%Pb	Sn-37wt%Pb
Orifice Diameter	100 μm	100 μm
Chamber Pressure	34.01 kPa	34.01 kPa
Crucible Pressure	170.07 kPa	170.07 kPa
Melt Temperature	533 K	523 K
Frequency	8.5 kHz	11.8 kHz

Table 2.1 Experimental conditions for Sn-25wt%Pb and Sn-37wt%Pb

Alloy	Sn-25wt%Pb	Sn-37wt%Pb
Droplet Diameter	183 ±4μm	179.5±1.5μm
Initial Velocity (N_2)	6.34 m/s	6.15 m/s
Initial Velocity (N_2-2%H_2)	6.62 m/s	6.05 m/s
Weight of Alloy	100 gm	100 gm

Master alloys of compositions Sn-25wt%Pb and Sn-37wt%Pb were prepared under the hood in the laboratory from 99.9% pure Sn and 99.9% pure Pb. The Sn and Pb were weighed, melted and cast in hemispherical ceramic cavities about 20 mm in diameter. The casts were then weighed and transferred to the crucibles. Table 2.1 shows the experimental conditions used during the experiments. Each experiment lasted between 200 and 300 seconds.

After each experiment, the weight of the collected powders in each calorimetric device was measured. The powders were then cleaned using acetone and allowed to dry in open air. They were cold mounted in 25.4 mm diameter plastic holders using room temperature curing epoxy and resin. The ratio of epoxy to resin was 9:1. The epoxy was allowed to solidify in the hood for one day. The samples (mounted powders in epoxy) were then cleaned with distilled water and methanol and dried. They were then ground using 260, 340, 400 and 600 grit papers and polished sequentially with 6 μm and 1 μm diamond paste, 0.3 μm alumina solution and 0.05 μm colloidal solution. Finally, each sample was etched for 12 to 15 seconds using one part nitric acid, one part acetic acid and eight parts glycerol. Three pictures were taken for each sample under an optical microscope; one each at magnifications of x100, x400 and x1000. The microstructures of the powders were investigated under each experimental condition and conclusions were made regarding the thermal state of the droplets and the morphologies of the droplets.

2.3.1 Determination of the shape of the solidification front within a droplet

Sn-5wt%Pb alloy powders collected at flight distances of 260 and 415.5 mm were investigated to study the shape of the solidification front inside the droplet. The powders were collected in oil in the in-situ calorimeter inside the uniform droplet generator. The powders were observed under the scanning electron microscope (SEM). Table 2.2 lists the experimental conditions under which the droplets were produced. 99.9%

Table 2.2 Experimental conditions for Sn-5wt%Pb

Alloy	**Sn-5wt%Pb**
Orifice Diameter	100 μm
Chamber Pressure	34.01 kPa
Crucible Pressure	170.07 kPa
Melt Temperature	553 K
Frequency	10.48 kHz
Droplet Diameter	180 μm

pure Sn-5wt%Pb alloy was used. The intercepted powders were cleaned with acetone and allowed to dry in air. They were cold mounted in 25.4 mm plastic holders using room temperature curing epoxy and resin. After they solidified, then were cleaned with distilled water and methanol. They were then ground using 340, 500, 1200 and 4000 grit papers and polished sequentially with 6 μm and 1 μm diamond paste, 0.3 μm alumina solution and 0.05 μm chromia solution. Finally each sample was etched for 12 to 15 seconds using one part nitric acid, one part acetic acid and eight parts glycerol. The powders were observed under a scanning electron microscope (SEM).

2.3.2 Determination of the enthalpy of the droplets in flight

The enthalpies of Sn-5wt%Pb droplets were measured as a function of flight distance. The droplets were collected in oil in the in-situ calorimeter inside the uniform droplet generator. The temperatures near the bottom and top of the oil were measured using a data acquisition system. These temperatures were used in an energy balance equation to determine the enthalpies of the droplets. Table 2.2 lists the system parameters that were used to measure the enthalpies of the droplets in flight. The enthalpies were measured at the following flight distances: 260, 415.5, 500, 550, 600, 612.4, and 650 mm

We used the procedure described in Section 2.2.1 to create the uniform droplets. Once the droplets were produced, we intercepted them in the oil baths at the required flight distances. Figure 2.7 shows a characteristic graph of the temperatures of the oil bath versus time for a given flight distance. The top curve shows the temperature registered by the thermocouple placed near the bottom of the oil bath and the bottom curve shows the temperature registered by the thermocouple placed near the surface of the oil bath. The two thermocouples initially show room temperature. As the droplets get collected in the oil bath, the temperatures start rising. This is because the heat

energy from the droplets is transferred to the calorimetric device. The time of the experiments ranges between 300 and 400 seconds. This is the time duration during which the droplets are collected in the oil bath in the calorimetric device. When the experiment stops, the temperatures start falling as a result of cooling. Cooling mainly occurs as a result of convection between the surface of the oil bath and the gas in the chamber. Radiation effects are neglected because the heat loss from the droplets by radiation is only a small fraction of the heat loss by convection. The next section explains the technique used to determine the enthalpy of the droplets from the temperatures of the oil bath.

Uniform droplets are collected in the oil bath while the experiment is in progress. H_d is the total enthalpy carried into the oil by the droplets. Some of it is transferred to the oil and to the droplets already in the oil. The rest of the enthalpy is lost to the atmosphere in the uniform droplet generator by either being absorbed by the walls of the calorimetric device or by being lost to the atmosphere through the walls and the surface of the calorimetric device. The total enthalpy loss is denoted by H_l.

The entire heat balance can be expressed by the following equation:

$$\frac{dH_d}{dt} - \frac{dH_l}{dt} = (m_d(t)\, c_d + m_o c_o(T))\frac{dT}{dt} \tag{2.1}$$

where m_d is the mass of the droplets collected in the oil in the calorimetric device, c_d is the specific heat of the droplets, m_o is the mass of the oil, c_o is the specific heat of the oil, T is the temperature and t is the time. m_d and c_o are functions of time and temperature, respectively.

The specific heat of the oil was measured as a function of temperature using a differential scanning calorimeter (DSC). The graph of the specific heat as a function of the temperature is shown in Figure 2.6. The curve fit result for the relationship between the specific heat and the temperature is given by the following equation:

$$c_o = 0.003T + 1.43 \tag{2.2}$$

The mass of the droplets m_d collected in oil changes with time. It can be measured using an electronic balance which has an error bar of ± 0.5 gm.

The enthalpy loss, H_l, through the calorimetric device was measured by running separate calibration experiments outside the system. Figure 2.3 shows a schematic diagram of the system that was used to run the calibration experiments. The system con-

sisted of the following parts: calorimetric device, oil, two thermocouples, heater, and data acquisition system. The calorimetric device, the amount of oil, the thermocouples, and the data acquisition system were the same as those used in the uniform droplet generator to carry out the actual experiments. As before, one thermocouple was placed near the bottom of the oil and the other thermocouple was placed near the surface of the oil. Details of these parts are described in Section 2.2. The heater was a 8 watts band resistance heater (Watlow Gordon). Using the circuit shown in Figure 2.3, electrical energy corresponding to the heat energy carried by the droplets was provided to the oil through the heater. Five separate experiments were carried out to cover the entire range of experimental conditions. In each experiment, a particular amount of electrical power was added to the oil. The data acquisition system captured the temperatures of the two thermocouples in the oil. The temperatures of both thermocouples were allowed to reach a steady state value. At steady state, the temperatures of the thermocouples showed no change. This implies that at steady state, the power input P_o into the oil was equal to the rate of enthalpy loss through the calibration system. This relationship can be expressed by the following equation:

$$\frac{dH_l}{dt} = P_o \tag{2.3}$$

Figure 2.4 shows the relationship between the rate of enthalpy loss and the temperature. A curve fit result shows that the relationship between the rate of enthalpy loss and the temperature is given by the following equation:

$$\frac{dH_l}{dt} = 0.111T - 3.057 \tag{2.4}$$

By substituting Equations 2.2, 2.4 and 2.5 into Equation 2.1, the following equation is obtained:

$$\frac{dH_d}{dt} = (m_d(t)\ (c_d + m_o(0.003T + 1.43)))\frac{dT}{dt} + (0.111T + 3.057) \tag{2.5}$$

By integrating Equation 2.5 with respect to time, the following expression is obtained:

$$\Delta H_d = \int_{T_i}^{T_f} (m_d(t)\, c_d + m_o\,(0.003T + 1.43))\, dT + \int_{t_i}^{t_f} (0.111T - 3.057)\, dt \tag{2.6}$$

where T_i is the initial temperature of the oil. This corresponds to the time t_i at the start of the experiment. T_f is the final temperature of the oil when the flow of droplets into the oil stops. This corresponds to the time t_f when the experiment stops. There are two ways to determine T_f. The first method is to read the temperature directly from the temperature-time chart. The second method is to determine a relationship between the rate of temperature loss as a function of temperature using a calibration technique. Then, a point corresponding to a linear part of the cooling curve can be picked. This point, along with t_f, can be used in the relationship to calculate T_f.

Equation 2.7 can be expressed in terms of temperature through the following equation. $\partial T/\partial t$ is the slope of the heating curve during the experiment. It captures the rate of temperature rise during the time when the droplets are collected in the oil.

$$\Delta H_d = \int_{T_i}^{T_f} \left(\frac{\partial m_d}{\partial t} c_d \frac{(T - T_i)}{\partial T/\partial t} + m_o\,(0.003T + 1.43)\right) dT + \int_{T_i}^{T_f} (0.111T - 3.057)) \frac{dT}{\partial T/\partial t} \tag{2.7}$$

The number of droplets collected in the oil bath is equal to the total mass of the droplets in the oil bath at the end of the experiment divided by the mass of an individual droplet. The mass of an individual droplet is equal to the product of its total volume and its density. This can be expressed as:

$$n = \frac{m_d}{V_d \cdot \rho_d} \tag{2.8}$$

where ρ_d is the density of the droplet and V_d is the volume of the droplet. Therefore, the enthalpy change of one droplet can be calculated by dividing the total enthalpy change of all the droplets by the total number of droplets collected. This expression is given by:

$$\Delta h_d = \frac{\Delta H_d}{n} \tag{2.9}$$

where Δh_d is the droplet enthalpy with the initial oil temperature (25°C) as the reference temperature. Equation 2.10 was used to calculate the enthalpy change of the droplet before and after impinging into the oil as a function of different flight distances from the orifice.

The computation of Δh_d for Sn-5wt%Pb droplets collected at a flight distance of 500 mm by using the Equations (2.1) - (2.9) is shown in Appendix I.

2.3.3 Determination of the undercooling of the droplets

This section qualitatively describes a procedure that can be used to evaluate the undercooling of the droplets from the enthalpy values of the droplets. Figure 2.5 shows a schematic graph that plots the enthalpy of each droplet as a function of flight distance at different undercooling levels [18]. This graph can be obtained theoretically by using a model [18, 24, 25] that determines the enthalpy of each droplet as a function of undercooling at different flight distances. In the absence of undercooling, the enthalpy values lie on the equilibrium line denoted by 3. Lines 1 and 2 correspond to different levels of undercooling. From the experimental procedure described in Section 2.3.2, the enthalpy of each droplet can be determined experimentally between a certain flight distance region in the uniform droplet generator. These values can then be plotted on Figure 2.5 and the range of the undercooling amount that the droplet acquires during the experiments can be determined.

More evidence of undercooling can be obtained by looking at the microstructures of the collected powders. In particular, two results in Chapter 3 show that the droplets are undercooled. They are as follows: we don't see any lamellar eutectic structures in the eutectic Sn-37wt%Pb alloys, and the primary phase in Sn-25wt%Pb and Sn-37wt%Pb is the Pb-rich phase.

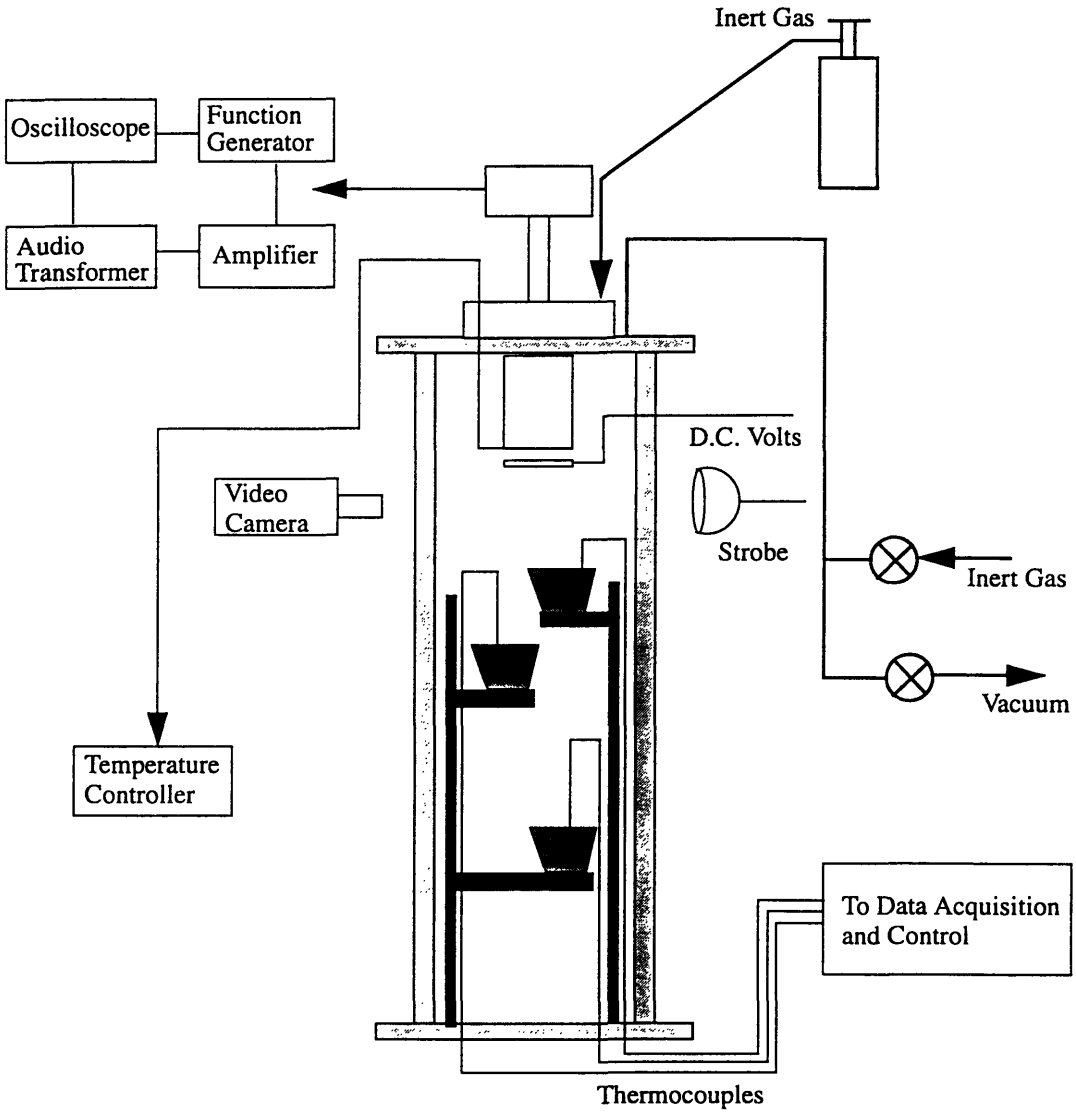

Figure 2.1 Schematic of the uniform droplet generator with the modular calorimetric apparatus.

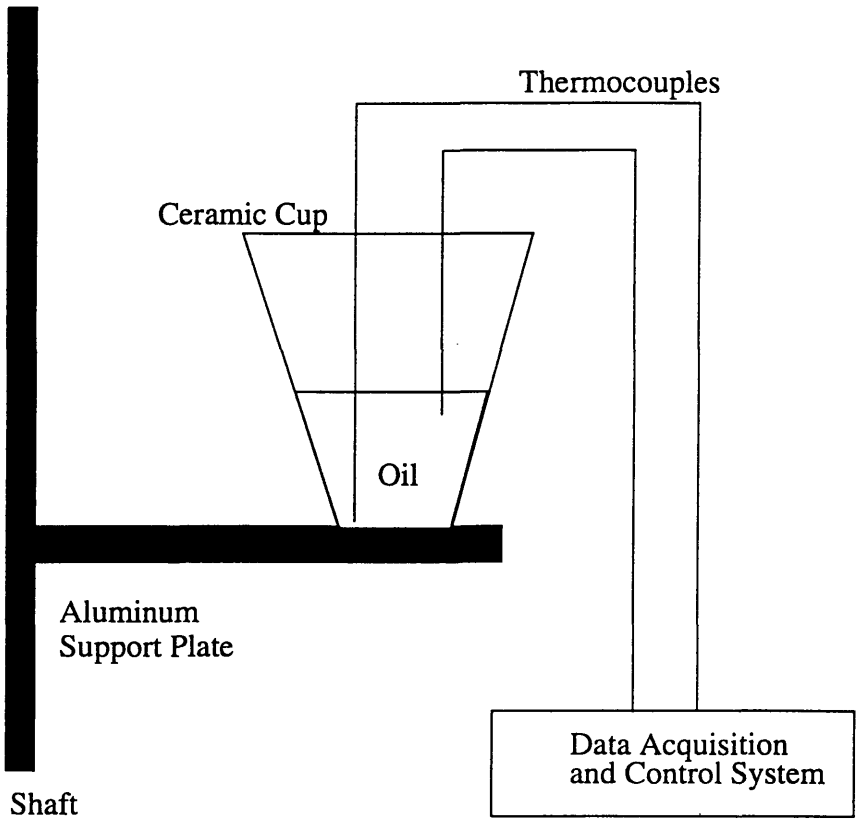

Figure 2.2 Schematic diagram of the calorimetric device.

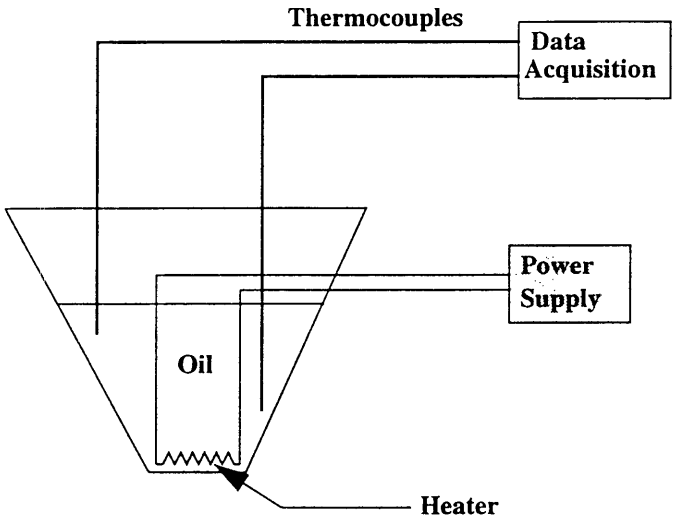

Figure 2.3 Schematic diagram of the calibration apparatus.

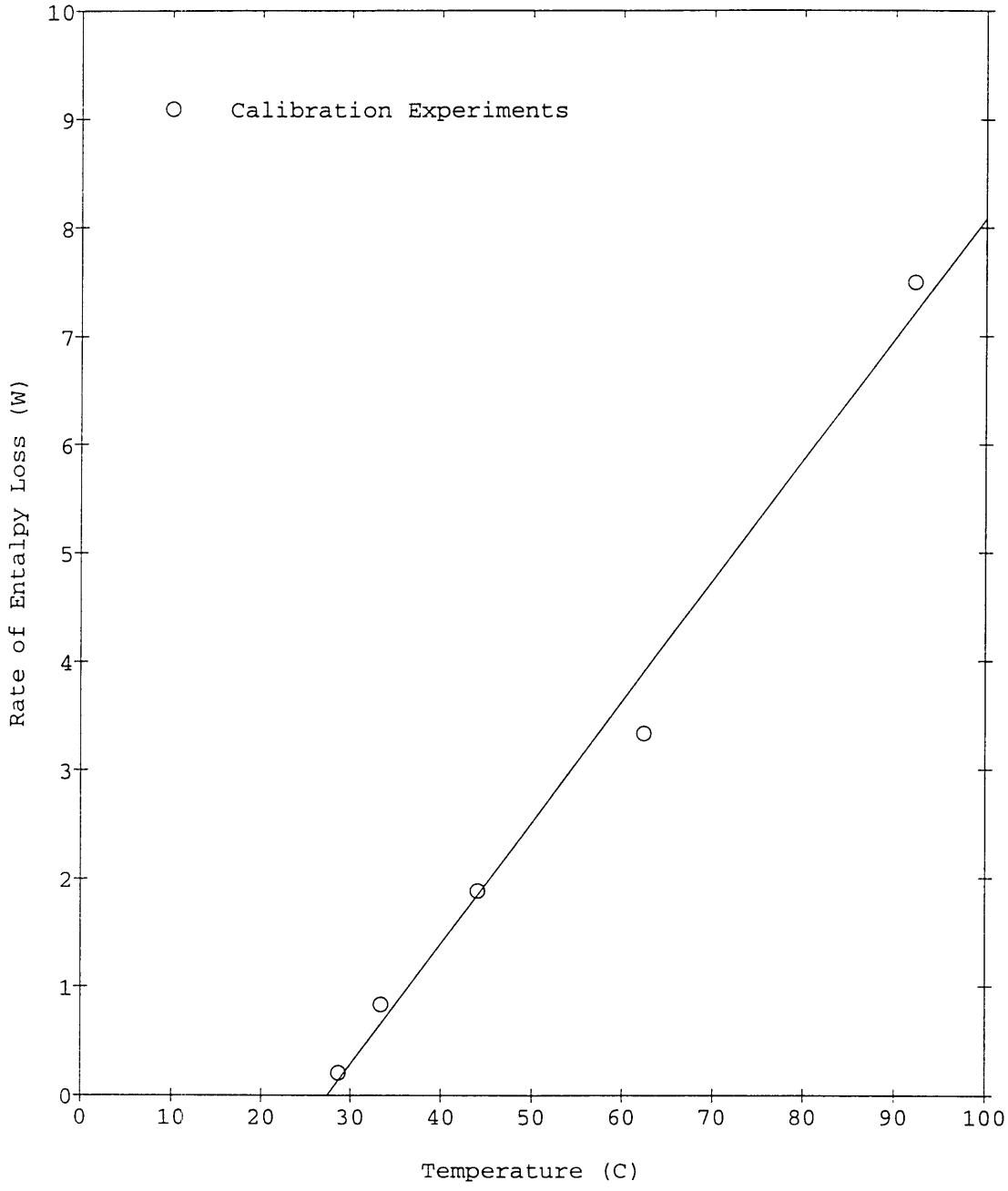

Figure 2.4 Rate of enthalpy loss plotted as a function of temperature during calibration experiments.

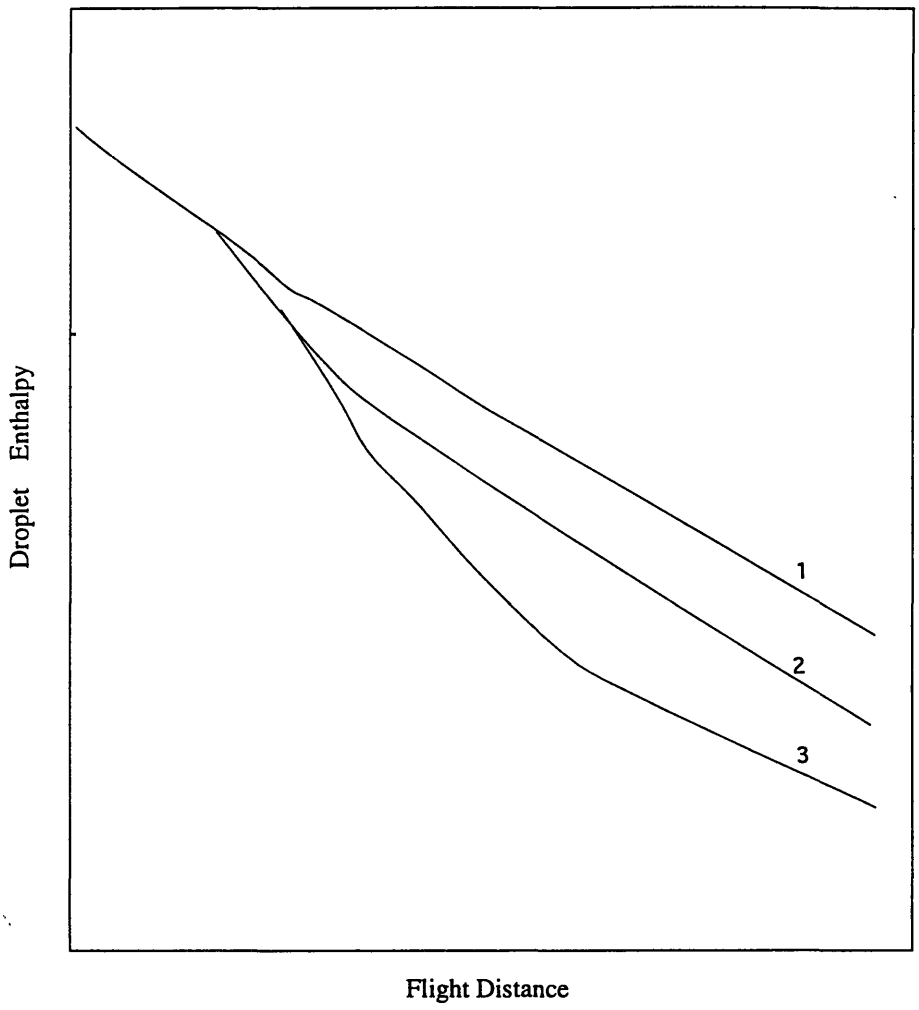

Figure 2.5 Schematic variation of the droplet enthalpies with flight distance at different levels of undercooling. The dotted curve denotes equilibrium solidification and the solid curves denote undercooling.

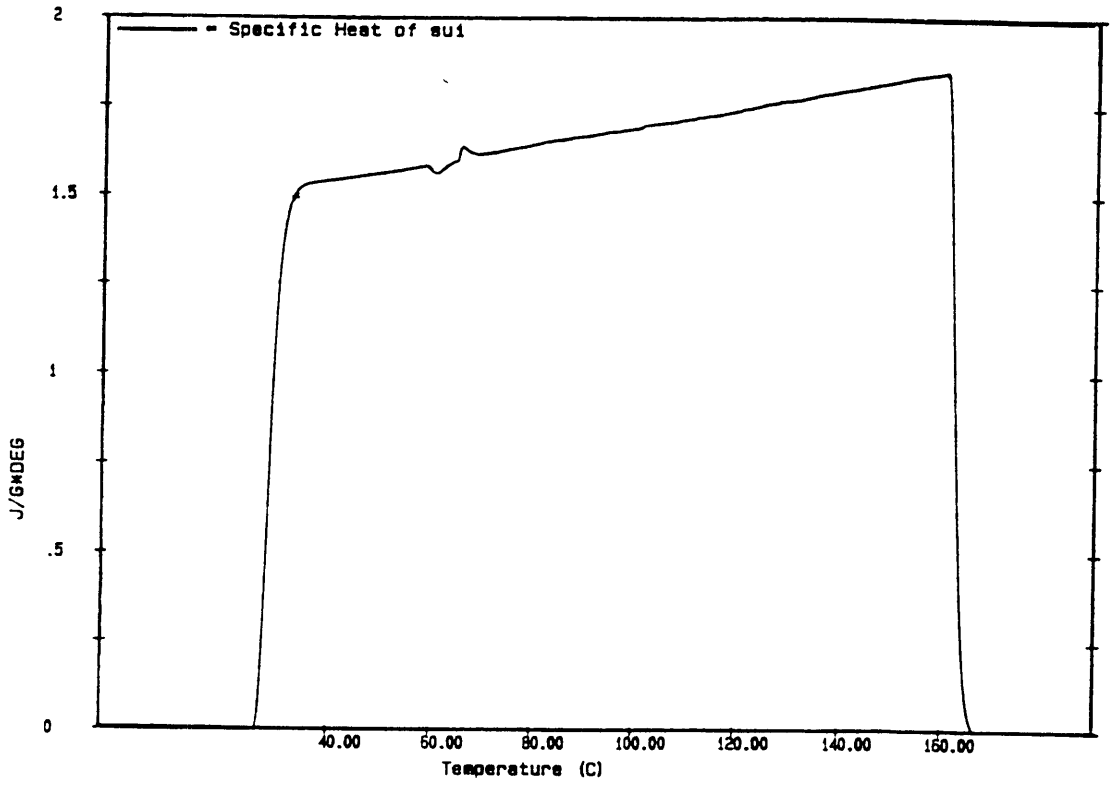

Figure 2.6 Specific heat of Dow Corning 704 oil as a function of temperature. Data obtained from Differential Scanning Calorimeter.

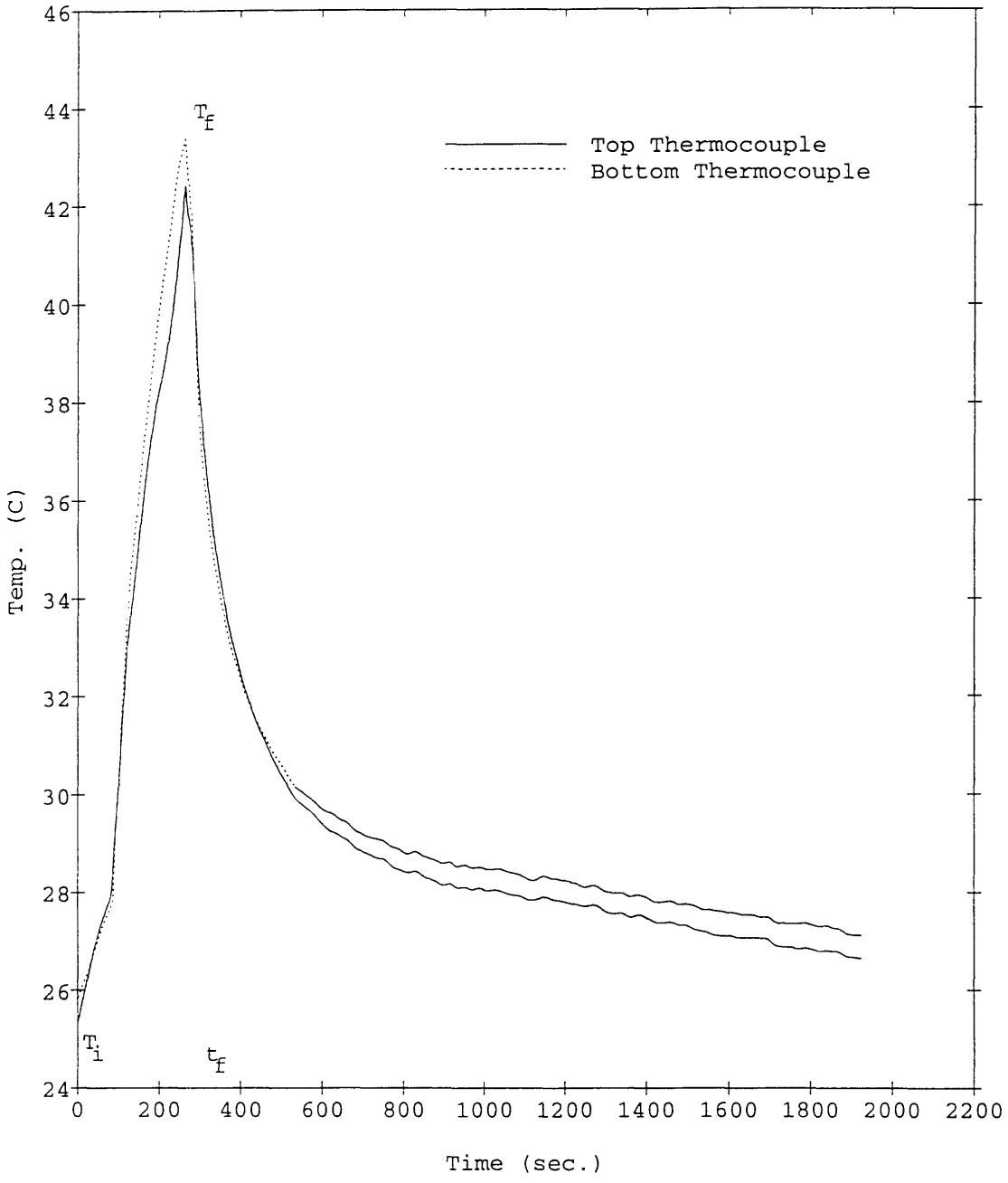

Figure 2.7 Temperatures near the bottom and top of the oil in the calorimetric device for Sn-5wt%Pb droplets collected in oil at 500 mm.

CHAPTER 3 Experimental Results

3.1 Relationship between the Thermal State of the Droplets and the Morphology of the Droplets

Under equilibrium solidification (without undercooling), the droplets start solidifying at their liquidus temperature and complete solidifying at their solidus temperature.Under equilibrium solidification, the thermal state of the droplets is defined by the temperature and liquid fraction of the droplets or the enthalpy and liquid fraction of the droplets. Under non-equilibrium solidification (with undercooling), the droplets start solidifying at a temperature lower then their liquidus temperature. The difference between the liquidus temperature and the temperature at which the droplets start solidifying is called the undercooling level. Under non-equilibrium solidification, the thermal state of the droplets is defined by the temperature, liquid fraction and initial undercooling of the droplets or the enthalpy, liquid fraction and undercooling of the droplets. During all the experiments, powders were collected in oil in the uniform droplet generator. The microstructures of the powders were observed under the microscope. The morphologies of the droplets were then deduced from the microstructures of the powders.

Figures 3.1 and 3.2 show the effects of temperature, enthalpy, and liquid fraction on the microstructures of the collected powders. The temperature, enthalpy, and liquid fraction were varied by changing the flight distance between the orifice and the substrate. We expect that as the flight distance from the orifice increases, the temperature, enthalpy, and liquid fraction of the droplets decrease. Figure 3.1 compares the microstructure of Sn-37wt%Pb powders collected in oil in the presence of N_2-2%H_2 gas at two different flight distances: 375 mm and 700 mm. The powders collected at 375 mm show a fine, dendritic microstructure with an irregular spherical shape. The powders at 700 mm show a somewhat coarser, two phase structure with a regular spherical shape. The difference in shape is due to the difference in the liquid fractions of the powders. The irregular spherical shape for the powders collected at a flight distance of 375 mm clearly indicates that these powders contained a higher level of liquid fraction than the powders collected at 700 mm which show a regular spherical shape. Therefore, the powders at 375 mm were deformed out of their regular spherical shape.

Figure 3.2 compares the microstructure of Sn-25wt%Pb powders collected in oil in the presence of N_2-2%H_2 gas at two different flight distances: 200 mm and 600 mm.

The powders collected at both distances are spherical. However, they are smaller in size at a flight distance of 200 mm. This is because the droplets at 200 mm are fully liquid with a high liquid fraction and cause each droplet to break up into smaller droplets on impact with the oil. The powders at 600 mm have a low liquid fraction and are not easily deformable. Therefore they retain their regular spherical shape. A measurement shows that the powders collected at 200 mm are about 1/4 the size of the powders collected at 600 mm.

Figure 3.3 shows the effect of undercooling of the droplets on the microstructure of the collected powders. The undercooling was varied by using two different inert gases in the uniform droplet generator. The two gases were N_2 and N_2-2%H_2. The use of N_2-2%H_2 enables the H_2 to react with the O_2 in the chamber. Therefore the potential for oxide to be formed on the surface of a molten alloy droplet which can then act as high potency heterogenous nucleation sites is reduced. Prevention of oxidation is considered to promote droplet undercooling. Hence the use of N_2-2%H_2 increases the chances for undercooling. Without H_2, however, oxidation can take place at oxygen potentials as low as $10^{-40} atm$ and thus could have readily occurred in the $CaSO_4$ desiccated N_2 gas. Therefore, the droplets produced in the N_2-2%H_2 gas were undercooled more than those produced in the N_2 gas. Figure 3.3 compares the microstructure of Sn-25wt%Pb powders collected in oil at a flight distance of 400 mm in N_2 and N_2-2%H_2 gases. The powders produced in N_2 froze mostly as they were as uniform spherical powders. The powders produced in N_2-2%H_2 solidified as irregular ellipsoids. The difference in shapes in due to the difference in the undercooling of the droplets in both the gases. The droplets produced in N_2-2%H_2 gas were undercooled more than the droplets collected in the N_2 gas due to the reasons mentioned in the previous paragraph. Therefore the start of solidification was delayed more in this case and therefore, these droplets contained more liquid than those produced in the N_2 gas for the same flight distance. The higher liquid fraction was responsible for deforming the droplets from their spherical shape in the N_2-2%H_2 gas. The powders produced in the two different gases also show a difference in their microstructure. In N_2-2%H_2, the powders show a fine-equiaxed microstructure, indicating a higher solidification rate for the powders produced in the N_2-2%H_2 gas. This condition suggests that these droplets were fully molten and undercooled when they impinged into the oil. The powders produced in N_2 show a coarser-dendritic microstructure, indicating a lower solidification rate for the powders produced in the N_2 gas.

Figure 3.4 shows the effect of alloy composition on the microstructure and shape of the powders. The alloy composition affects the undercooling of the droplets [16].

However, from the microstructures obtained in this work, it was difficult to correlate the composition of the alloy with the exact amount of undercooling of the droplets. Nevertheless, some significant differences were observed in terms of the liquid fraction of the collected powders. From the phase diagram in Figure 1.2, Sn-37wt%Pb is transformed into the solid stage from the liquid stage at a single temperature corresponding to the eutectic temperature. On the other hand, Sn-25wt%Pb goes through a region corresponding to the semi-solid phase before it is transformed into the solid stage. Therefore, the likelihood of deformation is higher in Sn-25wt%Pb than Sn-37wt%Pb since the former composition has a higher liquid fraction compared to the latter composition at any flight distance. This is indeed the trend observed in Figure 3.4. Figure 3.4 compares Sn-25wt%Pb powders with Sn-37wt%Pb powders at a flight distance of 400 mm in N_2-2%H_2 gas. The Sn-25wt%Pb powders show a higher degree of deformation in shape and have a finer microstructure. The Sn-37wt%Pb powders show a lower degree of deformation in shape and have a coarser-equiaxed morphology.

3.2 Initiation of the Solidification Front Inside the Droplet

The knowledge of the shape of the solidification front inside the droplets is essential for modeling the entire solidification process inside the droplets. Previous efforts have assumed that the shape of the solidification front inside the droplets has a planar configuration [20]. This assumes that the solidification front moves from one end of the droplet towards the other end. This assumption is mainly used to simplify the analysis since it is easier to model the planar configuration than any other solidification front geometry.

We hypothesize that in the uniform-droplet spray process, the solidification front has a spherical shape which initiates at the outer surface and moves radially inwards towards the center of the droplets. The droplet has the lowest temperature along its surface due to the heat transfer at the surface between the droplet and the atmosphere. The individual solidification fronts from the different nucleation sites that form near the surface eventually merge to form a hollow spherical solidification front inside the droplet. The solid ring grows and propagates towards the center of the droplet. To study the initiation of solidification, the microstructures of Sn-5wt%Pb droplets collected in oil in the calorimetric device were studied under the scanning electron microscope.

Figure 3.5 shows Sn-5wt%Pb droplets collected in oil at a flight distance of 415.5 mm. In all the droplets shown, a ring propagating towards the center is clearly visible.

This can probably be explained as the solidification zone expanding towards the center of the droplets. Figure 3.5 shows that the shape of the solidification front is spherical. This is expected since the droplets are exposed to the same conditions throughout their surface while travelling through the inert gas. Therefore the probability of nucleation sites being formed along the surface of the droplets is equal in all directions. This conclusion is supported by Figure 3.6.

Figure 3.6 shows Sn-5wt%Pb droplets collected in oil at a flight distance of 260 mm. The micrograph on the top shows a number of droplets mounted, ground and polished in an epoxy medium. It is conceivable that the white regions inside the droplets are the nucleation sites. A study of all the droplets in the medium shows that the solidification pattern within the droplet consists of several steps: nucleation sites are formed on the surface of the droplets, they grow in number and finally they merge together and form a solid ring that propagates towards the center of the droplets. By studying the different droplets shown in Figure 3.6, all the steps ranging from the origin of the nucleation sites along the surface of the droplets to the formation and propagation of the solid ring towards the center of the droplet can be identified. However, more work needs to be done in order to confirm these evidences.

3.3 Determination of the enthalpy of an individual droplet

Using the procedure outlined in Section 2.3, the enthalpies of Sn-5wt%Pb droplets were measured as a function of flight distance. The enthalpies were compared with the values calculated from an equilibrium solidification model. Table 3.1 lists the experimentally measured values and the equilibrium solidification model values. This section also describes how the experimentally measured values can be used to determine the undercooling of the droplets.

Table 3.1 Measured and Calculated Enthalpy Values

Flight Distance (mm)	Enthalpy Measurements from Experiments (J/droplet)	Enthalpy Calculations from Equilibrium Solidification Model (J/droplet)
260	1.60×10^{-3}	1.80×10^{-3}
415.5	1.50×10^{-3}	1.54×10^{-3}
500	1.21×10^{-3}	1.30×10^{-3}

Table 3.1 Measured and Calculated Enthalpy Values

Flight Distance (mm)	Enthalpy Measurements from Experiments (J/droplet)	Enthalpy Calculations from Equilibrium Solidification Model (J/droplet)
550	1.17×10^{-3}	1.18×10^{-3}
600	2.39×10^{-4}	1.05×10^{-3}
612.4	2.05×10^{-4}	1.01×10^{-3}
650	4.74×10^{-5}	9.25×10^{-4}

The enthalpies calculated using the equilibrium solidification model [19] are shown in the third column of Table 3.1. The model assumes that the droplets nucleate under equilibrium solidification conditions without undergoing any undercooling. The droplets start solidifying at their liquidus temperature and complete solidifying at their solidus temperature. The enthalpy of the droplets is determined by the temperature and amount of solidification of the droplets. This can be expressed by the following equation:

$$h_d = \oint_{25C}^{T} ((c \cdot dT) + xH_f)$$

or

$$h_d = xH_f + c\Delta T$$

where H_f is the enthalpy of fusion, c is the specific heat, and x is the liquid fraction. The enthalpy of the droplet is proportional to the liquid fraction of the droplet, which is to be expected since a higher liquid fraction means a higher temperature and a higher enthalpy.

Figure 3.7 presents the experimentally measured and the theoretically determined droplet enthalpies as a function of flight distance. In Figure 3.7, the circles represent the experimental data points whereas the triangles represents the equilibrium model predictions. There is a difference in the experimental values and the equilibrium model values, as expected. However, in order to determine the exact reasons for this discrepancy, more accurate experimental measurements need to be done. One of the probable

reasons for this discrepancy may be an overestimation of the heat loss during the calibration experiments. During the measurement of droplet enthalpies, we have used the steady state temperatures of the oil in the calorimetric device to measure the heat loss. However, the actual experiments in the uniform-droplet spray process are carried out during transient conditions. Therefore, there is an overestimation of the heat losses during the experimental measurements of the enthalpies. This might have led to an underestimation of the experimental enthalpies at all the flight distances.

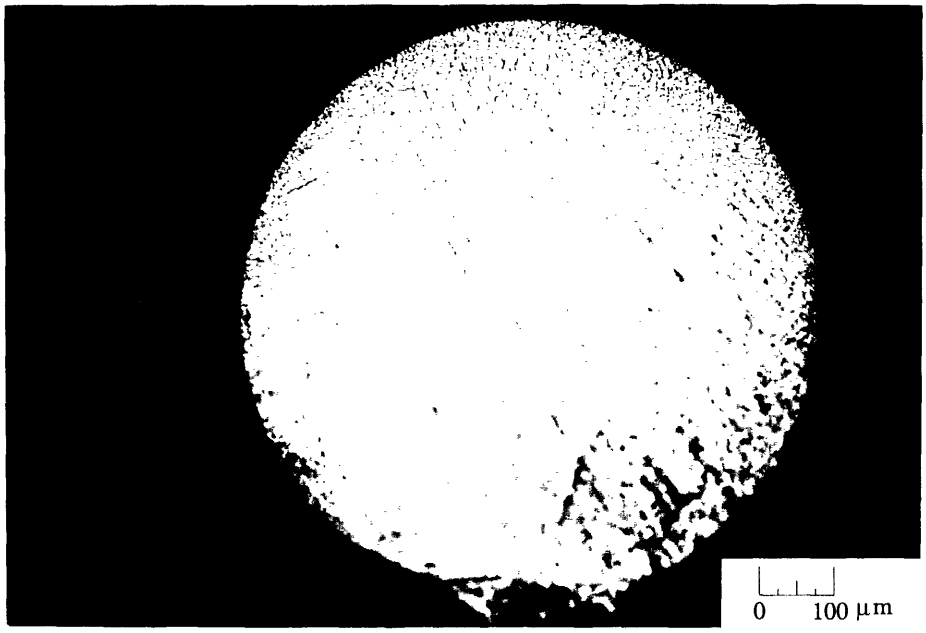

Sn-37wt%Pb (375 mm, N_2-2%H_2)

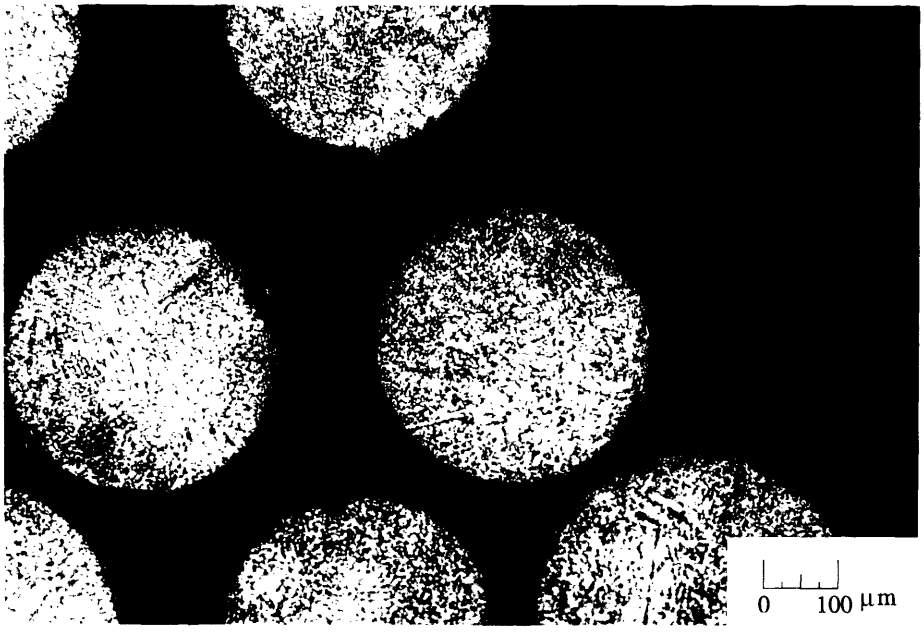

Sn-37wt%Pb (700 mm, N_2-2%H_2)

Figure 3.1 Sn-37wt%Pb droplets collected in oil in N_2-2%H_2 gas at 375 mm and 700 mm. The micrographs show the effects of temperature and liquid fraction on the microstructures of the collected powders.

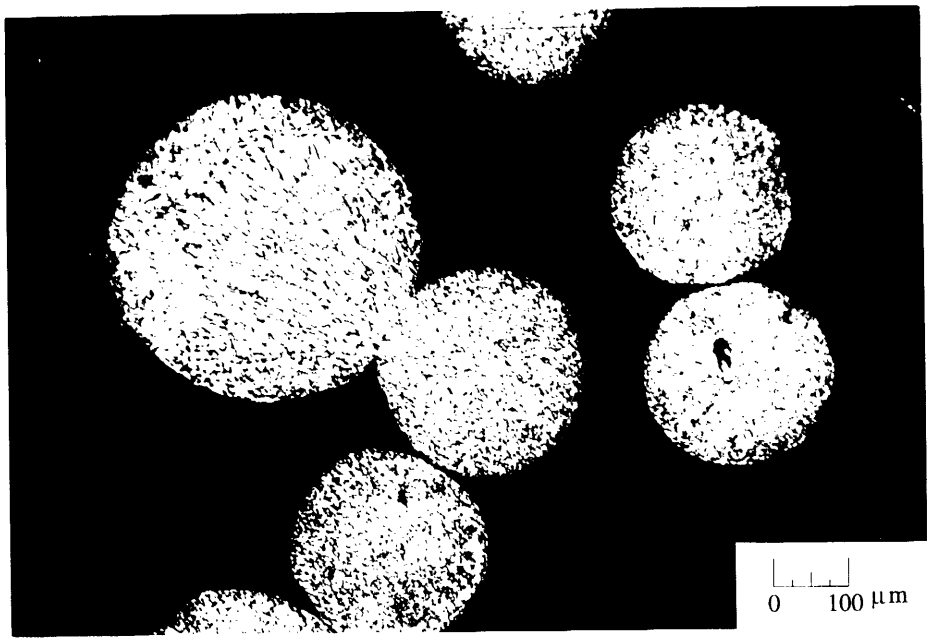

Sn-25wt%Pb (200 mm, N_2-2%H_2)

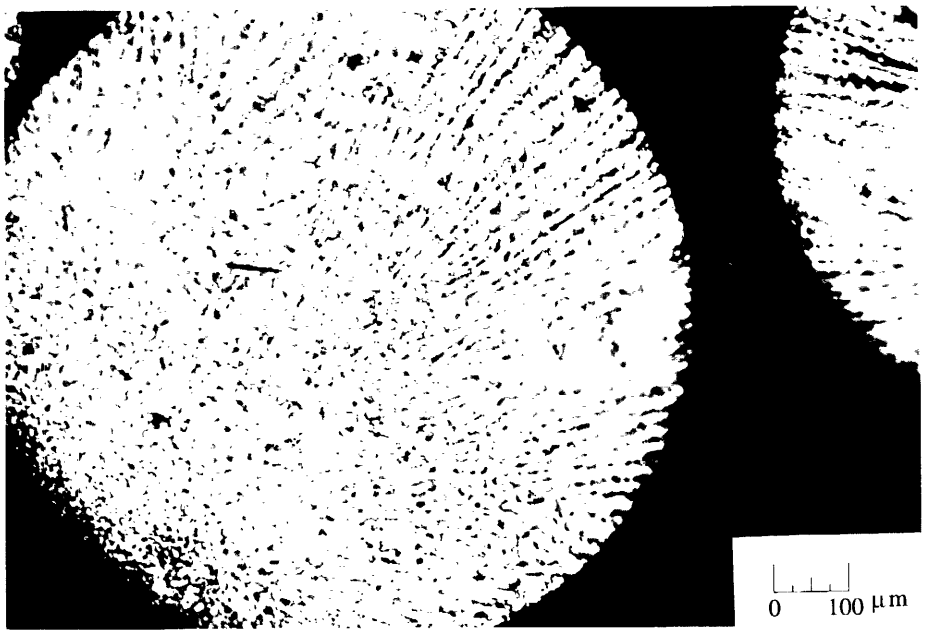

Sn-25wt%Pb (600 mm, N_2-2%H_2)

Figure 3.2 Sn-25wt%Pb droplets collected in oil in N_2-2%H_2 gas at 200 mm and 600 mm. The micrographs show the effects of temperature and liquid fraction on the microstructures of the collected powders.

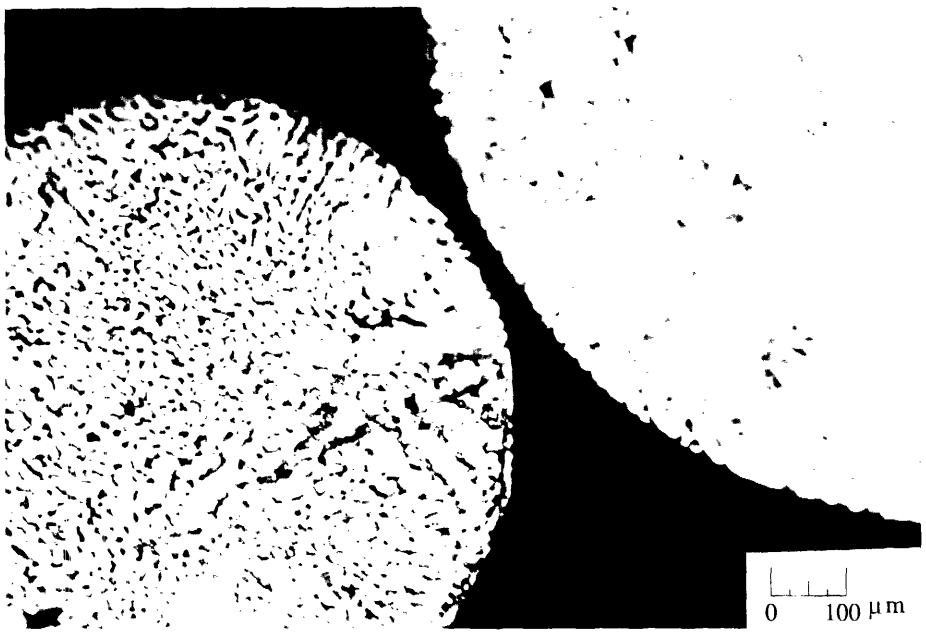

Sn-25wt%Pb (400 mm, N_2)

Sn-25wt%Pb (400 mm, N_2-2%H_2)

Figure 3.3 Sn-25wt%Pb droplets collected in N_2 gas and N_2-2%H_2 gas at 400 mm. The micrographs show the effect of undercooling on the microstructures of the collected powders.

Sn-25wt%Pb (400 mm, N_2-2%H_2)

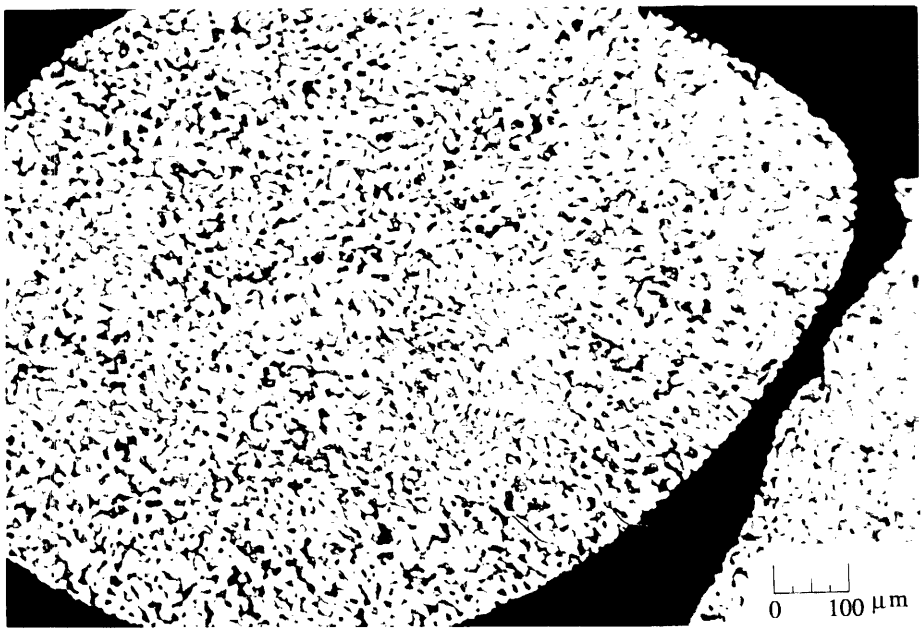

Sn-37wt%Pb (400 mm, N_2-2%H_2)

Figure 3.4 Sn-25wt%Pb droplets and Sn-37wt%Pb droplets collected in oil in N_2-2%H_2 gas at 400 mm. The micrographs show the effect of liquid fraction on the microstructures of the collected powders.

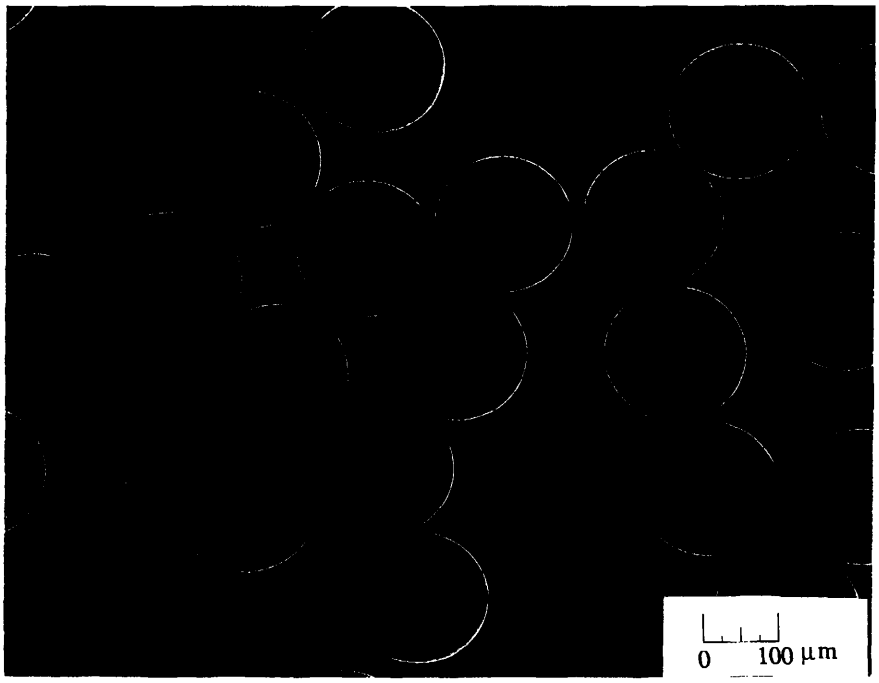

Sn-5wt%Pb (415.5 mm, N_2)

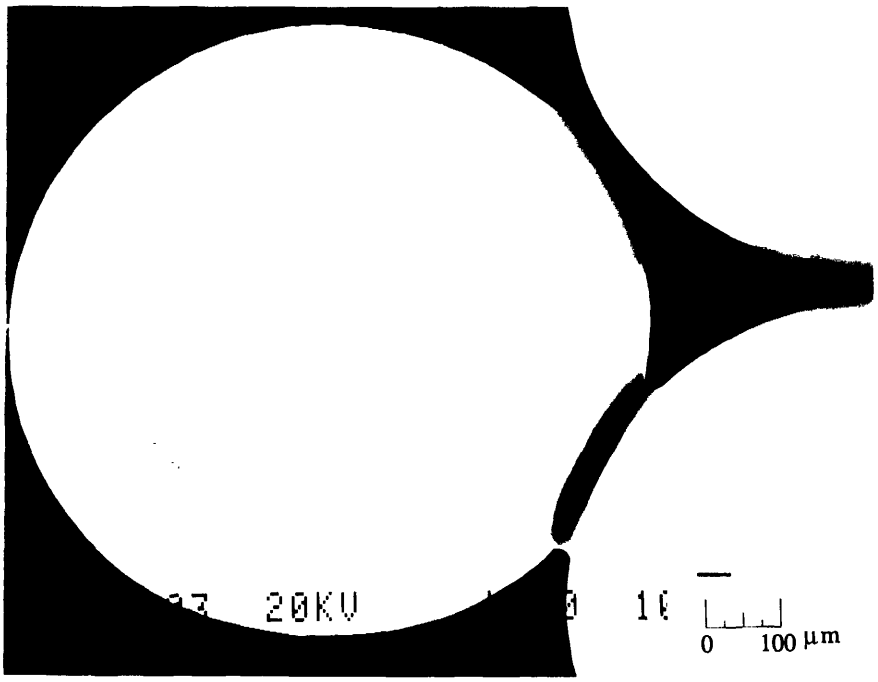

Sn-5wt%Pb (415.5 mm, N_2)

Figure 3.5 Sn-5wt%Pb droplets collected in oil in N_2 gas at 415.5 mm. The micrograph shows the shape of the solidification front inside the collected powders.

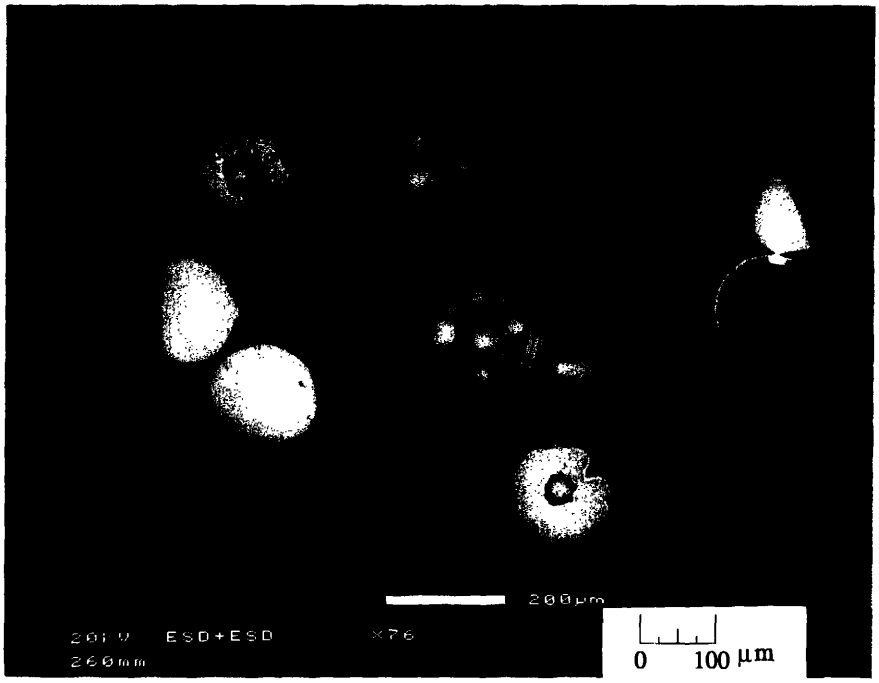

Sn-5wt%Pb (260 mm, N_2)

Sn-5wt%Pb (260 mm, N_2)

Figure 3.6 Sn-5wt%Pb droplets collected in oil in N_2 gas at 260 mm. The micrograph shows the initiation of solidification inside the collected powders.

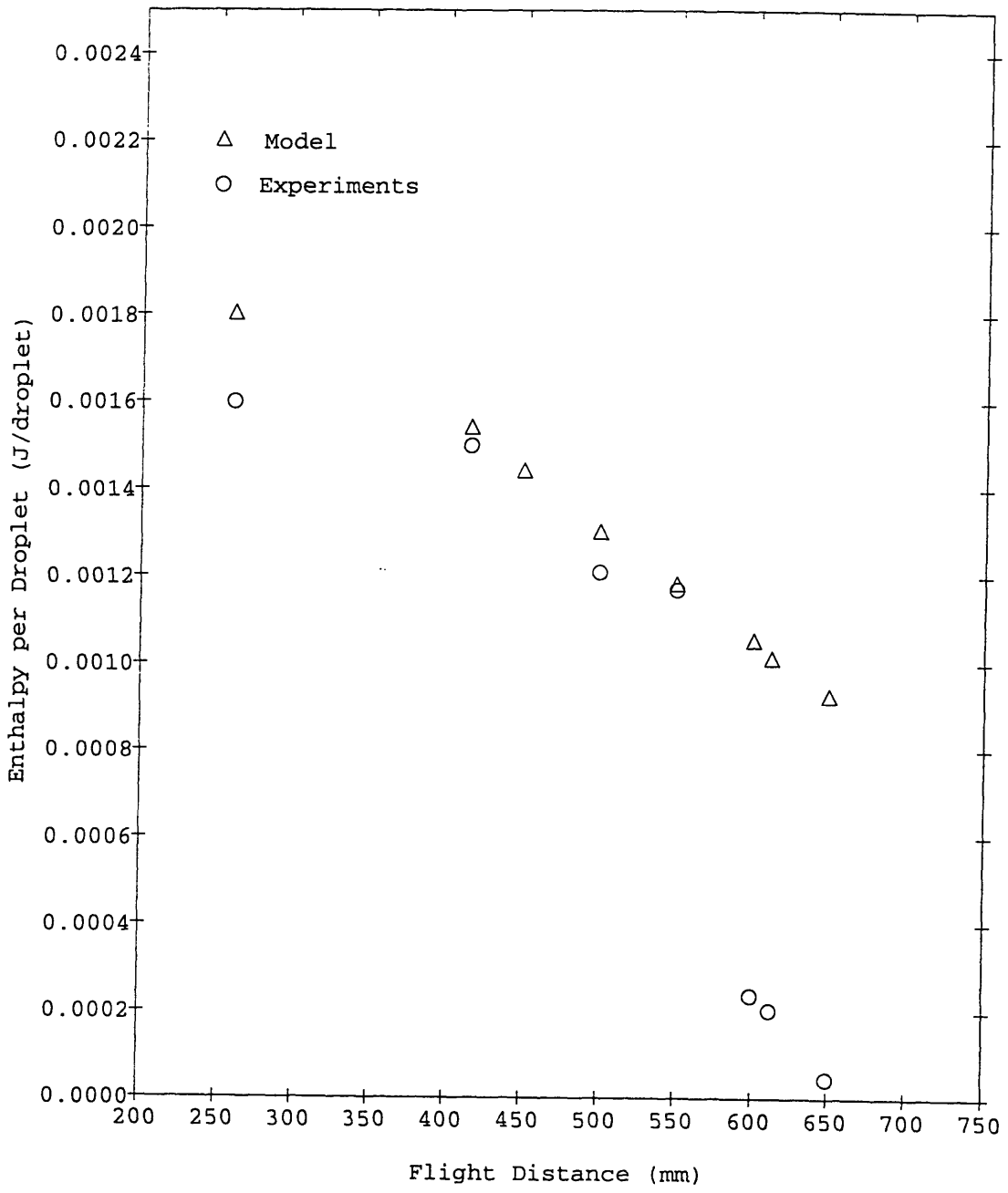

Figure 3.7 Variation of droplet enthalpy with flight distance. The circles represent the measured enthalpies and the line represents the equilibrium model prediction for Sn-5wt%Pb in N_2 atmosphere.

CHAPTER 4 Summary and Future Work

4.1 Summary

The uniform-droplet spray process is a droplet-based manufacturing process in which parts are made out of uniform molten metal droplets. The use of uniform droplets provides a number of advantages over conventional spray forming processes. The deposit has an equiaxed and homogenous microstructure with a low porosity. In order to maximize the potential of the uniform-droplet spray process, it is essential to characterize all the parameters that affect the microstructure of the deposit. This work studies various aspects of the thermal state of the droplets in the uniform-spray forming process.

The uniform droplets are collected in a calorimetric device that is built as a modular unit of the existing uniform-droplet apparatus where the uniform powders are created. The major aspects of the thermal state of the droplets that are studied are as follows: system variables that affect the thermal state of the droplets, relationships between the thermal state of the droplets and the microstructures of the collected powders, shape of the solidification front inside the droplets, and the enthalpy values of the individual droplets.

The main system variables that affect the thermal state of the droplets are flight distance, type of inert gas in the apparatus, and alloy composition. The flight distance affects the temperature, enthalpy, and liquid fraction of the powders. Powders collected at a smaller flight distance are deformed more because they contain a higher liquid fraction than the powders collected at a larger flight distance. The type of inert gas affects the undercooling of the powders. Powders collected in N_2-2%H_2 are undercooled more than the powders collected in N_2. The alloy composition affects the liquid fraction of the powders. Sn-25wt%Pb powders are deformed more than Sn-37wt%Pb powders because they contain a higher amout of liquid fraction at the same flight distance.

In order to determine solidification parameters inside the droplets, it is essential to have a knowledge of the shape of the solidification front inside the droplets. Previous studies have indicated that the shape of the solidification front is planar during the solidification of droplets in droplet-based manufacturing processes. However, from the observations in this work, the shape of the solidification front of the collected powders looks spherical. However, more work needs to be done in order to confirm this conclusion.

Finally, the enthalpies of the individual droplets in the uniform-droplet spray process are determined by using an energy balance equation that relates the enthalpies of the droplets to the heat losses that occur from the walls and surface of the calorimetric device. The measured droplet enthalpies range between 1.60×10^{-3} j/droplet and 4.74×10^{-5} j/droplet. These values are compared with values obtained from an equilibrium solidification model. The enthalpies in the model range between 1.80×10^{-3} j/droplet and 9.25×10^{-4} j/droplet.

4.2 Future Work

To predict internal solidification parameters in an undercooled droplet, a model is currently being developed [18]. This model is a modification of the LGK model developed by Lipton, Glicksman and Kurz [20]. The LGK model is suitable for free dendritic growth in an undercooled binary alloy melt. It permits the calculation of the growth rate and interfacial concentrations for small undercooling under equilibrium conditions.The modified model can predict the temperature, enthalpy, solid-liquid interface velocity, solid-liquid interface composition and dendritic tip radius inside a highly undercooled droplet. The assumptions underlying this model are as follows:

1. This model is capable of predicting dendritic growth in a highly undercooled melt. In this case, the solid-liquid interface migrates at a very high velocity. This restricts diffusional rearrangement of the atoms at the interface, forcing the interfacial concentrations to deviate from local equilibrium values. The high interface velocity forces the kinetic partition ratio to become greater than the equilibrium kinetic partition ratio.
2. The dendritic tip shape is assumed to be paraboloid of revolution.
3. The heat and mass transport occur by diffusion only.
4. Local equilibrium is maintained at the solid-liquid interface.

We believe that the droplets in our system undergo undercooling. This is due to the large discrepancy observed between the experimental and equilibrium model enthalpy values for large flight distances. However, we are not aware of the amount of undercooling that the droplets go through. The total undercooling consists of four different kinds of undercooling: curvature, constitutional, thermal and kinetic. The kinetic undercooling is a measure of the deviation of the kinetic partition from the equilibrium kinetic partition. It is significant at high solid-liquid interface velocities. The total undercooling can be expressed in the form of an equation consisting of three unknown quantities: dendritic tip radius, solutal Peclet number and kinetic partition ratio. By

using a morphological stability criterion, a second equation giving a relationship between the dendritic tip radius and the solutal Peclet number is obtained. From a previously developed model by Aziz [18] which is used to describe solidification in an undercooled dilute binary alloy, a third equation giving a relationship between the kinetic partition ratio and the solutal Peclet number is determined. Therefore, for a given level of undercooling, the three equations can be simultaneously solved for the dendritic tip radius, the solutal Peclet number and the kinetic partition ratio. Furthermore, the solutal Peclet number is related to the interface velocity and the kinetic partition ratio is related to the interface concentration. The interface velocity is related to the liquid fraction, the temperature and the enthalpy.

Therefore, the modified model can predict the internal solidification parameters inside a highly undercooled droplet as a function of the undercooling level. These parameters include the temperature, enthalpy, liquid fraction, solid-liquid interface velocity, the solid-liquid interface concentration, and dendritic tip radius.

Bibliography

[1] Rayleigh, F.R.S. 1878. "On the Instability of Jets." Proceedings of the London Mathematic Society. 10 (4): 4-13.

[2] Schneider, J.M. and C.D. Hendricks. 1964. "Source of Uniform-Sized Liquid Droplets." Review of Scientific Instruments. 35 (10): 1349-1350.

[3] Pimbley, W.T. and H.C. Lee. 1977. "Satellite Droplet Formation in a Liquid Jet." IBM Journal of Research and Development. 21: 21-30.

[4] Evans, R.W., A.G. Leatham, and R.G. Brooks. 1985. "The Osprey Preform Process." Powder Metallurgy. 28 (1): 12-20.

[5] Lavernia, E.J. and N.J. Grant. 1988. 'Spray Deposition of Metals: A Review." Materials Science and Engineering. 98: 381-394.

[6] Gutierrez-Miravete, E.J. Lavernia, G.M. Trapaga, J. Szekely, and N.J. Grant. 1989. "A Mathematical Model of the Spray Deposition Process." Metallurgical Transactions A. 20A: 71-85.

[7] Lavernia, E.J. 1989. "Evolution of Microstructure During Spray Atomization and Deposition." International Journal of Rapid Solidification. 5: 47-85.

[8] Mathur, P., D. Apelian, and A. Lawley. 1988. "Analysis of the Spray Deposition Process." Acta Metallurgy. 37 (2): 429-443.

[9] Mathur, P.C. 1988. "Analysis of the Spray Deposition Process." Ph.D. Thesis. Drexel University.

[10] Trapaga-Martinez, L.G. 1990. "Gas-Particle-Deposit Interactions During Plasma Spraying and Spray Forming Processes." Sc.D. Thesis. Massachusetts Institute of Technology.

[11] Garrity, E.D. 1989. "A Phenomenological Analysis of Droplet Impact During Spray Deposition." Ph.D. Thesis. Drexel University.

[12] Bewlay, B.P. 1987. "Spray Forming of Alloys." Ph.D. Thesis. Oxford University.

[13] Annavarapu, S., R.D. Doherty, D. Apelian, A. Lawley, and P. Mathur. 1990. "Fundamental Aspects of Consolidation and Microstructure Development During Spray Casting." Presented at the International Conference on Spray Forming held at Swansea U.K. on September 17-19, 1990.

[14] Choudhary, K. C., L.G. Redekopp and T. Maxworthy. 1980. "The Nonlinear Capillary Instability of a Liquid jet." Journal of Fluid Mechanics. 96 (part 2): 257-297.

[15] Cooper, K.P., I.E. Anderson, and J.H. Perepezko. 1981. "Crystallization of Undercooled Pb-Sn Alloys." Proceedings of the 4th International Conference on Rapidly Quenched Metals. Sendai.

[16] Chu, M.G., Y. Shiohara, and M.C. Flemings. 1984. "Solidification of Highly Undercooled Sn-Pb Alloy Droplets." Metallurgical Transactions A. 15A: 1303-1310.

[17] Ando, T., J.H. Chun, and S. Sahu. 1993. "In-Flight Solidification of Uniform Droplets of Sn-25wt.%Pb and Sn-40wt.%Pb Alloys. Presented at the Third International Conference on Powder Metallurgy Conference held at Kyoto, Japan, 1993.

[18] Ando, T. 1993. "Modeling of Dendritic Solidification in a Highly Undercooled Droplet." Boston University. Private Communications.

[19] Passow, C.H. 1992. "A Study of Spray Forming using Uniform Droplet Sprays, M..S. Thesis. Massachusetts Institute of Technology.

[20] Kurz, W., and D.J. Fisher. 1989. "Fundamentals of Solidification." Trans Tech Publications, Third Edition.

[21] Heinzl, J., and C.H. Hertz. 1985. "Ink-Jet Printing." Advances in Electronics and Electron Physics. 65: 91-171.

[22] Raghavan, V. 1983. "Physical Metallurgy: Principles and Practise." Prentice-Hall Publications, 1983.

[23] Reed-Hill, R. E., and R. Abbaschian. 1992. "Physical Metallurgy Principles." PWS Kent Publishing Company, Third Edition.

[24] Boettinger, W.J., S. R. Corriel, and R. Trivedi. 1988. "Rapid Solidification Processing: Principles and Technologies, ods. R. Mehrabian and P.A. Parrish, Claitur's Publishing Division, 1988, pp13.

[25] Lipton, L., W. Kurz, and R. Trivedi. 1987. Acta Metallurgy. 99: 957.

Appendix I

This appendix calculates the enthalpy change of an individual Sn-5wt%Pb droplet before and after it impinges into the oil. The droplets are collected at a flight distance of 500mm. The appendix first describes the conditions of the experiment. The enthalpy change is computed by using the equations derived in section 2.3. Figure A1.1 shows the temperatures of the thermocouples near the bottom and top of the calorimetric device during the collection of Sn-5wt%Pb droplets in oil.

Experimental Conditions:

alloy	Sn-5wt%Pb
flight distance	500 mm
mass of oil, m_o	1.52 gm
specific heat of oil at 25°C, c_o	1.47×10^{-3} J/gm-mm
mass of droplets collected in oil, m_d	2.10 gm
specific heat of droplets collected in oil, c_d	0.213×10^{-3} J/gm-mm
initial temperature at the start of the experiment, T_i (figure A1.1)	25.2 °C
final temperature at the end of the experiment, T_f (figure A1.1)	43.47 °C
duration of experiment, t_f (figure A1.1)	274.5 seconds
slope of the heating curve, $\partial T/\partial t$ (figure A1.1)	0.211 °C/second
number of droplets collected in oil, n	8.6×10^4 droplets
rate of collection of droplets in oil, $(\partial m_d) / (\partial t)$	0.00765 gm/second

Equation 2.8 derived in section 2.3 is used to compute the total enthalpy change of all the droplets collected in oil. This is expressed by:

$$\Delta H_d = \int_{T_i}^{T_f} \left(\frac{\partial m_d}{\partial t} c_d \frac{(T - T_i)}{\partial T / \partial t} + m_o (0.00255T + 1.43) \right) dT + \int_{T_i}^{T_f} (0.111455T - 3.057142) \frac{dT}{\partial T / \partial t} \tag{A1.1}$$

By substituting the values from the experimental conditions, ΔH_d is calculated to be 104.06 J.

Equation 2.10 derived in section 2.3 is used to compute the enthalpy change of an individual droplet. This expression is given by:

$$\Delta h_d = \frac{\Delta H_d}{n} \tag{A1.2}$$

By using equation A1.2, Δh_d is calculated to be 1.21×10^{-3} J/droplet.

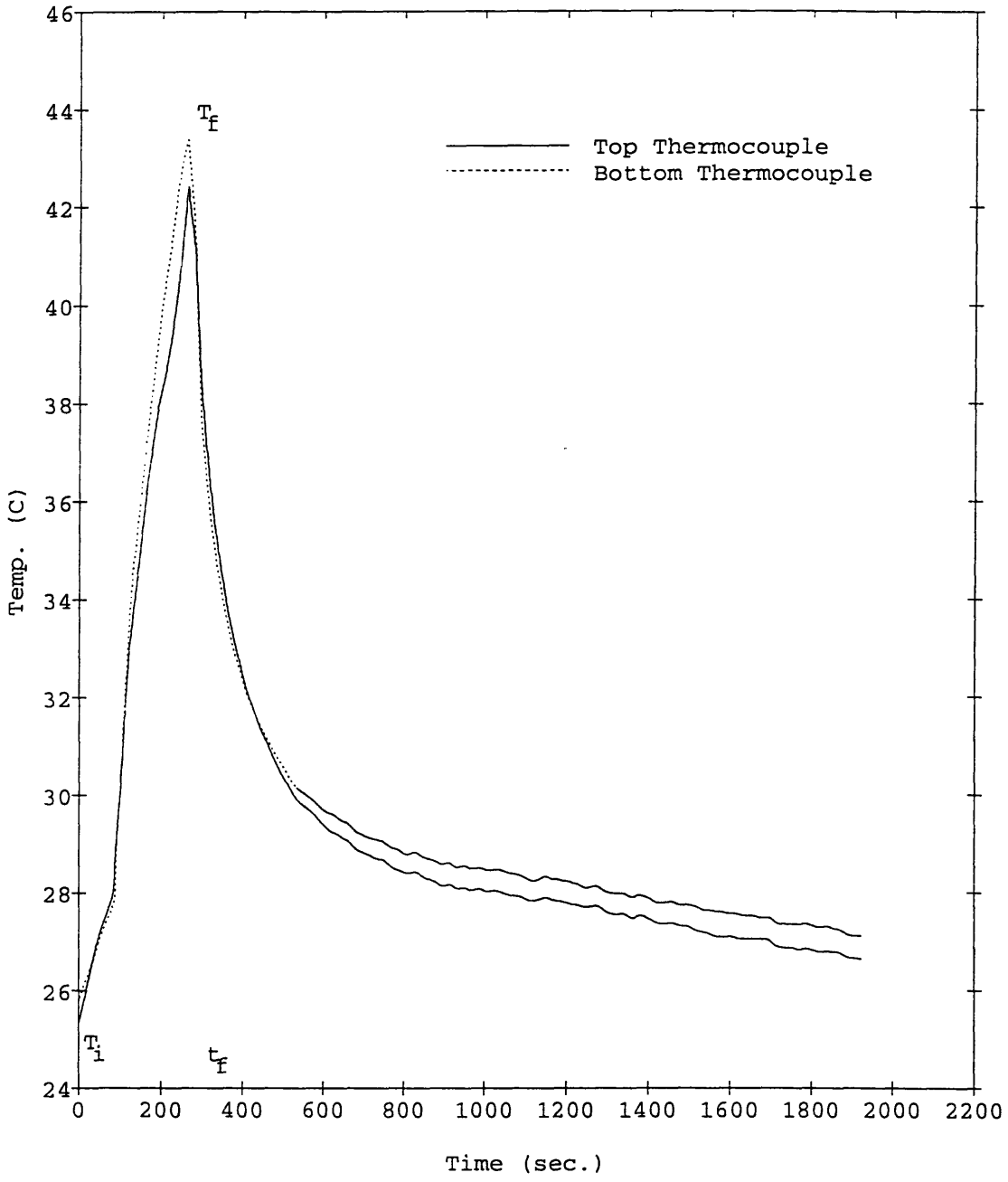

Figure A1.1 Temperatures near the bottom and top of the oil in the calorimetric device during the collection of Sn-5wt%Pb droplets in oil. The calorimetric device was located at a flight distance of 500 mm.